Supporting Information

Dehydropolymerization of $H_3B{\cdot}NMeH_2$ using a $[Rh(DPEphos)]^+$ catalyst: the promoting effect of $NMeH_2$.

Gemma M. Adams,[a] David E. Ryan,[a] Nicholas A. Beattie,[b†] Alasdair I. McKay,[a] Guy C. Lloyd–Jones[c] and Andrew S. Weller.*[a]

[a] Chemistry Research Laboratories, Mansfield Road, University of Oxford, Oxford, OX1 3TA, UK
[b] Institute of Chemical Sciences, Heriot Watt University, Edinburgh, EH14 4AS, UK
[c] School of Chemistry, University of Edinburgh, Edinburgh, EH9 3FJ, UK
[†] Present Address: School of Chemistry, University of Manchester, Oxford Road, Manchester, M13 9PL, UK

Corresponding Author Email Address: andrew.weller@chem.ox.ac.uk

Coordination Modes of Xantphos–iPr, Xantphos–Ph and DPEphos

Xantphos–^{i}Pr, Xantphos–Ph and DPEphos show different spreads of coordination modes as shown by the crystallographically characterized examples contained in the Cambridge Structural Database (as of August 2018).[14–16] The M–O distances and P–M–P angles of these complexes are detailed in Figure S1 and show that Xantphos–^{i}Pr has the greatest propensity for *mer*–κ^3–POP coordination (85% of 54 examples), whilst DPEphos is most likely to exist in a *cis*–κ^2–PP conformation (93% of 290 complexes). Interestingly, Xantphos–Ph appears to be an intermediate between these two coordination extremes, with 69% of its 223 complexes reported to be *cis*–κ^2–PP, whilst 19% are *mer*–κ^3–POP ligated. These coordination preferences may influence the mechanism of $H_3B{\cdot}NMeH_2$ dehydropolymerization.

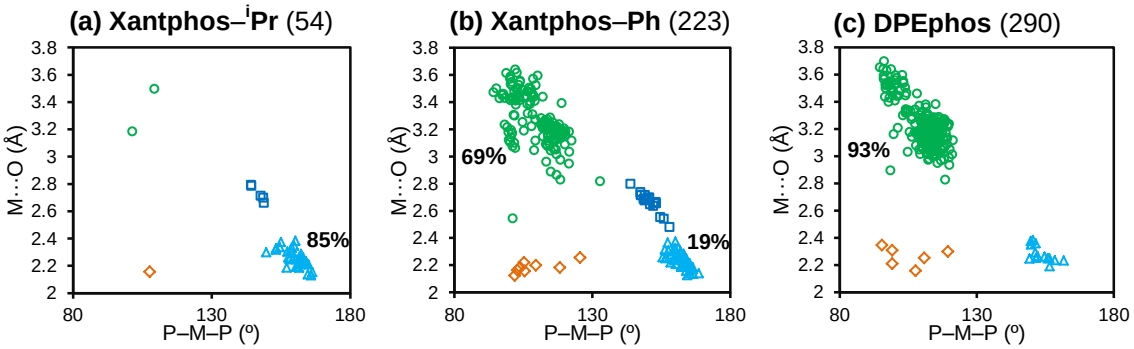

Figure S1. Plot of M–O distance (Å) vs P–M–P bite angle (°) in crystallographically characterized transition metal complexes containing **(a)** Xantphos–^{i}Pr (54 complexes), **(b)** Xantphos–Ph (223 complexes) and **(c)** DPEphos (290 complexes). Number of complexes examined in parentheses. Ligand coordination geometries as follows: ○ = *cis*–κ^2–PP; □ = *trans*–κ^2–PP; △ = *mer*–κ^3–POP; ◇ = *fac*–κ^3–POP.

Experimental

All manipulations, unless otherwise stated, were performed under an argon atmosphere using standard Schlenk line and glovebox techniques. Glassware was oven dried at 130°C overnight and flame dried under vacuum prior to use. Pentane, hexane, Et_2O and CH_2Cl_2 were dried using a Grubbs–type solvent purification system (MBraun SPS–800) and degassed by three successive freeze–pump–thaw cycles.[1] THF was dried over Na/benzophenone, vacuum distilled, degassed by three successive freeze–pump–thaw cycles and stored over 3.0 Å molecular sieves. 1,2–$F_2C_6H_4$ (pre–treated with alumina) and CD_2Cl_2 were dried over CaH_2, vacuum distilled, degassed by three successive freeze–pump–thaw cycles and stored over 3.0 Å molecular sieves. $H_3B{\cdot}NMe_3$ was purchased from Sigma–Aldrich and sublimed prior to use (5.0×10^{-2} mbar, 298 K). $H_3B{\cdot}NMeH_2$ was purchased from Boron Specialities and recrystallized twice from Et_2O at −18°C. Hg (99.9995%) was purchased from Sigma–Aldrich, washed with 1,2–$F_2C_6H_4$ and dried in vacuo prior to use. 3,3–dimethyl–1–butene was purchased from Sigma–Aldrich, dried over Na, vacuum distilled and stored over 3.0 Å molecular sieves. PPh_3 was purchased from Sigma–Aldrich and used as received. DPEphos was purchased from Strem Chemicals and used as received. $BH_3{\cdot}THF$ (1.0 M in THF) and $NMeH_2$ (2.0 M in THF) were purchased

from Fisher Scientific and used as received to form solutions in THF solvent of the desired concentrations. $Na[BAr^F_4]$ (Ar^F = 3,5–$(CF_3)_2C_6H_3$),[2] $[BH_2(NMeH_2)_2][BAr^F_4]$,[3] $D_3B{\cdot}NMeH_2$,[4] $H_3B{\cdot}NMeD_2$,[4] [Rh(DPEphos)(NBD)][BAr^F_4] (**1a**),[5] [Rh(DPEphos)(η^6–o–xylene)][BAr^F_4] (**7**),[6] Rh(Xantphos–^{i}Pr)$(H)_2Cl$,[7] [Rh(Xantphos–Ph)(η^2–$H_2B(NMe_3)(CH_2)_2{}^t$Bu)][BAr^F_4] (**A**),[8] and $[Rh(Ph_2P(CH_2)_3PPh_2)(C_6H_5F)][BAr^F_4]$[9] were prepared by literature methods. $[Rh(NBD)_2][Al(OC(CF_3)_3)_4]$ was prepared according to the literature procedure for $[Rh(COD)_2][Al(OC(CF_3)_3)_4]$.[10]

NMR spectra were recorded on a Bruker AVIIIHD 500 or Bruker AVIIIHD 400 nanobay spectrometer at room temperature, unless otherwise stated. Residual protio solvent was used as a reference for ^{1}H NMR spectra in deuterated solvent samples. For NMR spectrometric samples in 1,2–$F_2C_6H_4$ or protio−THF solvent, or a mixture of both, ^{1}H NMR spectra were pre–locked to a sample of C_6D_6 (25%) and 1,2–$F_2C_6H_4$ (75%) and referenced to the centre of the downfield solvent multiplet, δ = 7.07 and 3.57 respectively. ^{31}P and ^{11}B NMR spectra were referenced against 85% H_3PO_4 (external) and $BF_3{\cdot}OEt_2$ (external) respectively. Chemical shifts (δ) are quoted in ppm and coupling constants (*J*) in Hz. ESI–MS (electrospray ionization mass spectrometry) of organometallic complexes were recorded using a Bruker MicrOTOF instrument directly connected to a modified Innovative Technology glovebox. The mass spectrometer was calibrated in positive ion mode using a 10.0 ng mL^{-1} mixture of tetraalkylammonium bromide salts $[N(C_nH_{2n+1})_4]Br$ (n = 2 – 8, 12, 16, 18) in CH_2Cl_2. Typical experimental acquisition parameters were: sample flow rate, 4.0 µL min^{-1}; nebulizer gas pressure, 0.4 bar; drying gas (argon) at 60°C flowing at 4.0 L min^{-1}; capillary voltage, 4.5 kV. The solvents used were 1,2–$F_2C_6H_4$ or CH_2Cl_2. Samples were diluted to a concentration of approximately 1.0 × 10^{-6} M and filtered (0.2 µm pore size) before running. Elemental microanalyses were performed by Stephen Boyer at London Metropolitan University.

Gel permeation chromatography (GPC) was performed on a Malvern Viscotek GPCmax chromatograph fitted with a refractive index (RI) detector. The triple-column (plus guard column) setup was contained within an oven (35°C) and consisted of a porous styrene divinylbenzene copolymer with a maximum pore size of 1,500 Å. THF containing 0.1% w/w $[N^nBu_4]Br$ was used as the eluent at a flow rate of 1.0 mL min^{-1}. Samples were dissolved in the eluent (2.0 mg mL^{-1}), filtered (0.2 µm pore size) and run immediately. The calibration was conducted using a series of monodisperse polystyrene standards (M_n = 474 – 476,800 g/mol) obtained from Sigma–Aldrich.

*Synthesis of [Rh(DPEphos)(NBD)][Al(OC(CF$_3$)$_3$)$_4$] (**1b**)*

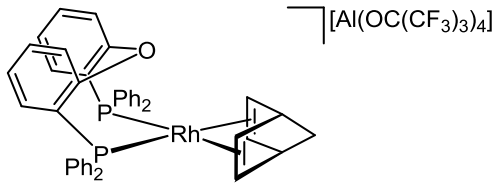

1b

A solution of DPEphos (129.0 mg, 239.5 µmol) in 1,2–$F_2C_6H_4$ (10.0 mL) was added dropwise to a Schlenk flask containing a solution of [Rh(NBD)$_2$][Al(OC(CF$_3$)$_3$)$_4$] (300.0 mg, 239.2 µmol) in 1,2–$F_2C_6H_4$ (8.0 mL). The resulting orange solution was left to stir for 12 hours. The solution was filtered, concentrated to ca. 3.0 mL under vacuum, layered with pentane (40.0 mL) and left to crystallize for ca. 48 hours at room temperature. Following removal of the supernatant by filtration, the dark orange crystalline material was washed with pentane (10.0 mL × 3) and dried under vacuum. Yield: 350.0 mg (206.0 µmol, 86%).

^{1}H NMR (400 MHz, CD_2Cl_2, 298 K): δ 7.55 – 7.31 (m, 22 H, aryl CH), 7.07 – 6.10 (m, 6 H, aryl CH), 4.30 (s, br, 4 H, NBD–HC=CH), 3.85 (s, br, 2 H, NBD–CH), 1.53 (s, 2 H, NBD–CH_2). **^{31}P{^{1}H} NMR** (162 MHz, CD_2Cl_2, 298 K): δ 17.0 (d, $^1J_{RhP}$ 159). **ESI–MS** (1,2–$F_2C_6H_4$, 60˚C, 4.5 kV): *m/z* 733.13 (calculated 733.13 for the [Rh(DPEphos)(NBD)]$^+$ fragment, showing the correct isotope pattern). **Elemental Microanalysis**: Calc. ($C_{59}H_{36}Al_1F_{36}O_5P_2Rh_1$): C, 41.67; H, 2.13. Found: C, 41.76; H, 2.23.

*Synthesis of [Rh(DPEphos)(η^2–$H_2B(NMe_3)(CH_2)_2{}^tBu$)][BAr$^F{}_4$] (**2a**)*

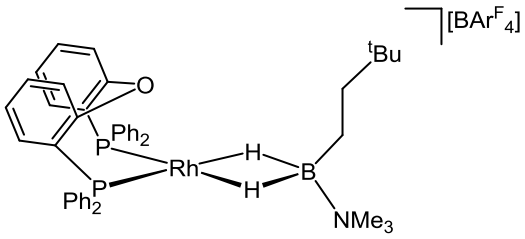

2a

[Rh(DPEphos)(NBD)][BAr$^F{}_4$] (**1a**) (547.2 mg, 342.7 µmol) and $H_3B{\cdot}NMe_3$ (32.0 mg, 438.7 µmol) were dissolved in 1,2–$F_2C_6H_4$ (5.0 mL) in a J. Young flask. The mixture was immediately frozen in liquid N_2 and hydrogenated. On warming to room temperature, the mixture was shaken, yielding a dark blue solution, forming [Rh(DPEphos)($H_3B{\cdot}NMe_3$)][BAr$^F{}_4$] in situ.[11] The solution was rapidly degassed with three successive freeze–pump–thaw cycles and placed under an atmosphere of argon. 3,3–dimethylbut–1–ene (0.3 mL, 2327.7 µmol) was added to the J. Young flask, and a further 3.0 mL of 1,2–$F_2C_6H_4$ was added to ensure all of the 3,3–dimethylbut–1–ene had entered the reaction mixture. The reaction mixture was stirred for 90 minutes, turning from dark blue to purple in colour. The solution was filtered; the solvent removed in vacuo and the resultant purple powder was washed with hexane (10.0 mL × 3), and dried under vacuum. Yield: 452.5 mg (272.3 µmol, 79%). A small number of purple crystals of **2a** could be obtained by recrystallization from CH_2Cl_2/pentane at −20°C, however these were not suitable for single crystal X–ray diffraction studies.

^{1}H NMR (500 MHz, CD_2Cl_2, 298 K): δ 7.72 (s, br, 8 H, $[BAr^F{}_4]^-$–ortho–CH), 7.56 (s, br, 4 H, $[BAr^F{}_4]^-$–para–CH), 7.45 – 7.28 (m, 22 H, aryl CH), 7.13 (d, 2 H, $^2J_{HH}$ 8, aryl CH), 6.87 (t, 2 H, $^2J_{HH}$ 8, aryl CH), 6.63 (m, 2 H, aryl CH), 2.59 (s, 9 H, NMe_3), 1.49 (m, 2 H, $CH_2C\underline{H_2}^tBu$), 0.78 (s, 9 H, ^{t}Bu), 0.49 (m, 2 H, $C\underline{H_2}CH_2{}^tBu$), −5.55 (br, 2 H, RhH_2B). Upon decoupling to ^{11}B, the resonance at δ −5.55 sharpened slightly. **^{11}B NMR** (160 MHz, CD_2Cl_2, 298 K): δ 33.3 (s, br, RhH_2B), −6.6 (s, $[BAr^F{}_4]^-$). **^{31}P{^{1}H} NMR** (202 MHz, CD_2Cl_2, 298 K): δ 40.0 (d, $^1J_{RhP}$ 180). **ESI–MS** (CH_2Cl_2, 60˚C, 4.5 kV): *m/z* 798.22 (calculated 798.27 for the $[Rh(DPEphos)(\eta^2–H_2B(NMe_3)(CH_2)_2{}^tBu)]^+$ fragment, showing the correct isotope pattern). **Elemental Microanalysis**: Calc. ($C_{77}H_{64}B_2F_{24}N_1O_1P_2Rh_1$): C, 55.65; H, 3.88; N, 0.84. Found: C, 55.78; H, 3.95; N, 0.82.

*Synthesis of $[Rh_2(DPEphos)_2(\mu–H)(\mu–H_2B{=}NHMe)][BAr^F{}_4]$ (**3a**)*

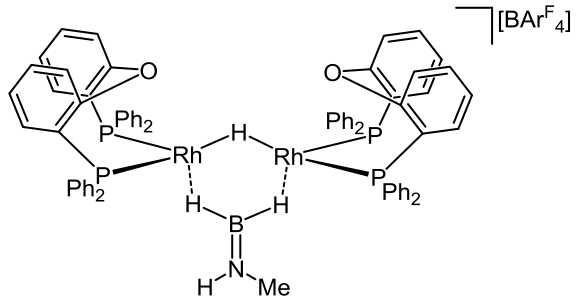

3a

$[Rh(DPEphos)(NBD)][BAr^F{}_4]$ (**1a**) (35.0 mg, 21.9 μmol) and $H_3B{\cdot}NMeH_2$ (2.0 mg, 44.6 μmol) were dissolved in 1,2–$F_2C_6H_4$ (0.35 mL) in a high pressure J. Young NMR tube. The sample was immediately frozen in liquid N_2 and hydrogenated. On warming to room temperature, the mixture was shaken, and the light orange solution turned darker in colour. The sample was immediately placed into the NMR spectrometer.

Selected spectrometric data: **^{1}H NMR** (500 MHz, 1,2–$F_2C_6H_4$, 298 K): δ 8.33 (s, br, 8 H, $[BAr^F{}_4]^-$–ortho–CH), −9.12 (br, 1 H, $Rh_2(\mu–BH_2)$ and $Rh_2(\mu–H)$). Upon decoupling to ^{31}P, the resonance at δ −9.12 sharpened. Note that the resonance at δ −9.12 is expected to integrate 1.5 H relative to the resonance at δ 8.33, due to the concomitant formation of $[BH_2(NMeH_2)_2][BAr^F{}_4]$.[12] **^{11}B NMR** (160 MHz, 1,2–$F_2C_6H_4$, 298 K): δ 55.8 (br, RhH_2B), −6.3 (s, $[BAr^F{}_4]^-$), –7.1 (t, $^1J_{BH}$ ~120, $[BH_2(NMeH_2)_2]^+$). **^{11}B{^{1}H} NMR** (160 MHz, 1,2–$F_2C_6H_4$, 298 K): δ 55.8 (br, RhH_2B), −6.3 (s, $[BAr^F{}_4]^-$), −7.1 (s, c **^{31}P{^{1}H} NMR** (202 MHz, 1,2–$F_2C_6H_4$, 298 K): δ 28.3 (d, $^1J_{RhP}$ 150). **ESI–MS** (1,2–$F_2C_6H_4$, 60˚C, 4.5 kV): *m/z* 1326.20 (calculated 1326.20 for the $[Rh_2(DPEphos)_2(\mu–H)(\mu–H_2B{=}NHMe)]^+$ fragment, showing the correct isotope pattern). These NMR and ESI−MS spectrometric data are analogous to the well–studied $PR_2(CH_2)_3PR_2$ (R = Ph, ^{i}Pr) analogues of complex **3a**,[12] thereby enabling characterization.

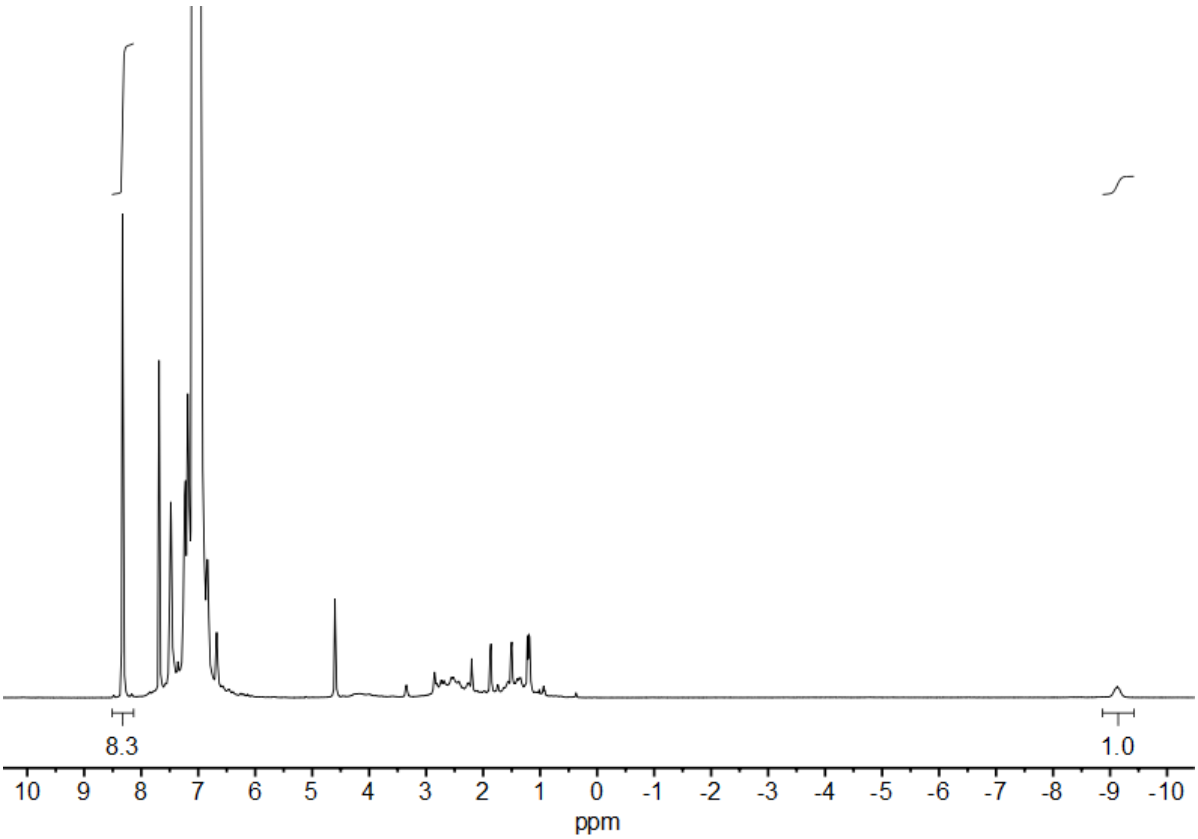

Figure S2. In situ ^{1}H NMR spectrum (1,2–$F_2C_6H_4$ solvent, 298 K) of the reaction mixture forming $[Rh_2(DPEphos)_2(\mu\text{–}H)(\mu\text{–}H_2B{=}NHMe)][BAr^F{}_4]$ (**3a**).

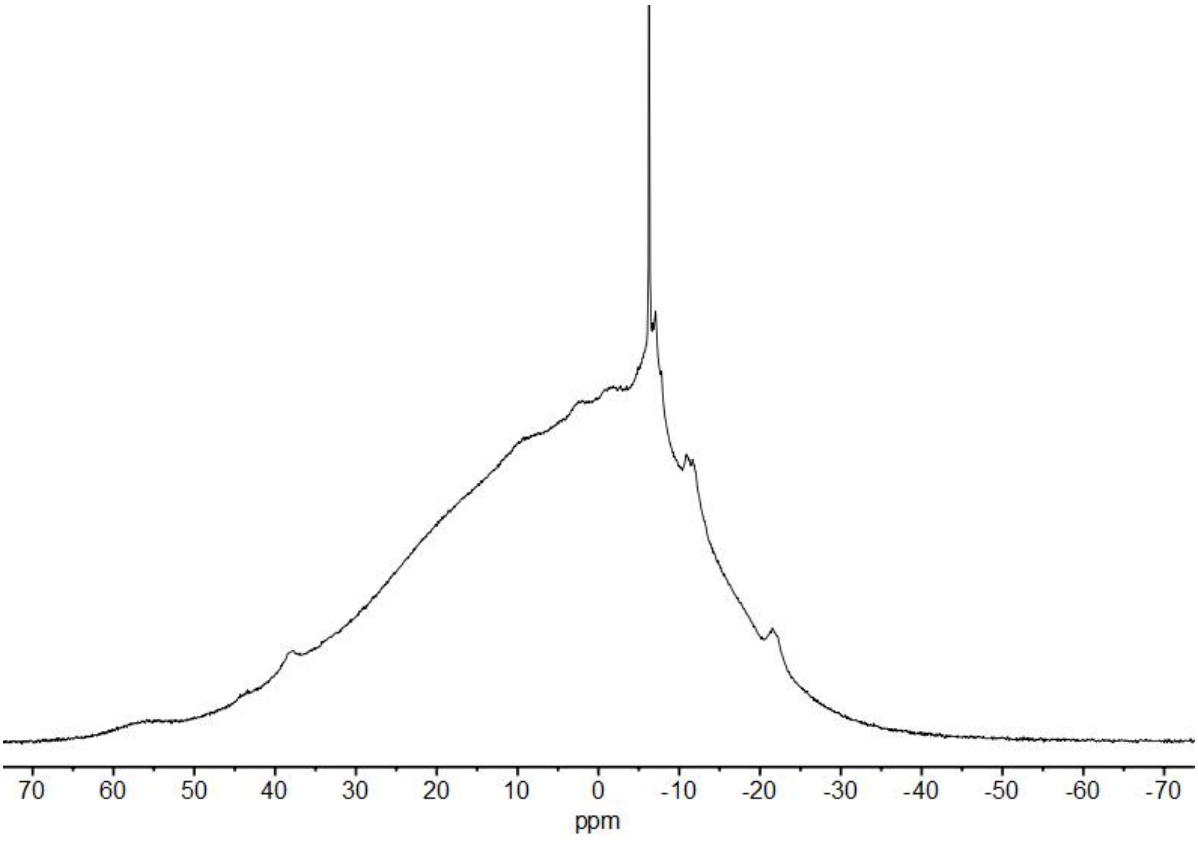

Figure S3. In situ ^{11}B NMR spectrum (1,2–$F_2C_6H_4$ solvent, 298 K) of the reaction mixture forming $[Rh_2(DPEphos)_2(\mu\text{–}H)(\mu\text{–}H_2B{=}NHMe)][BAr^F{}_4]$ (**3a**).

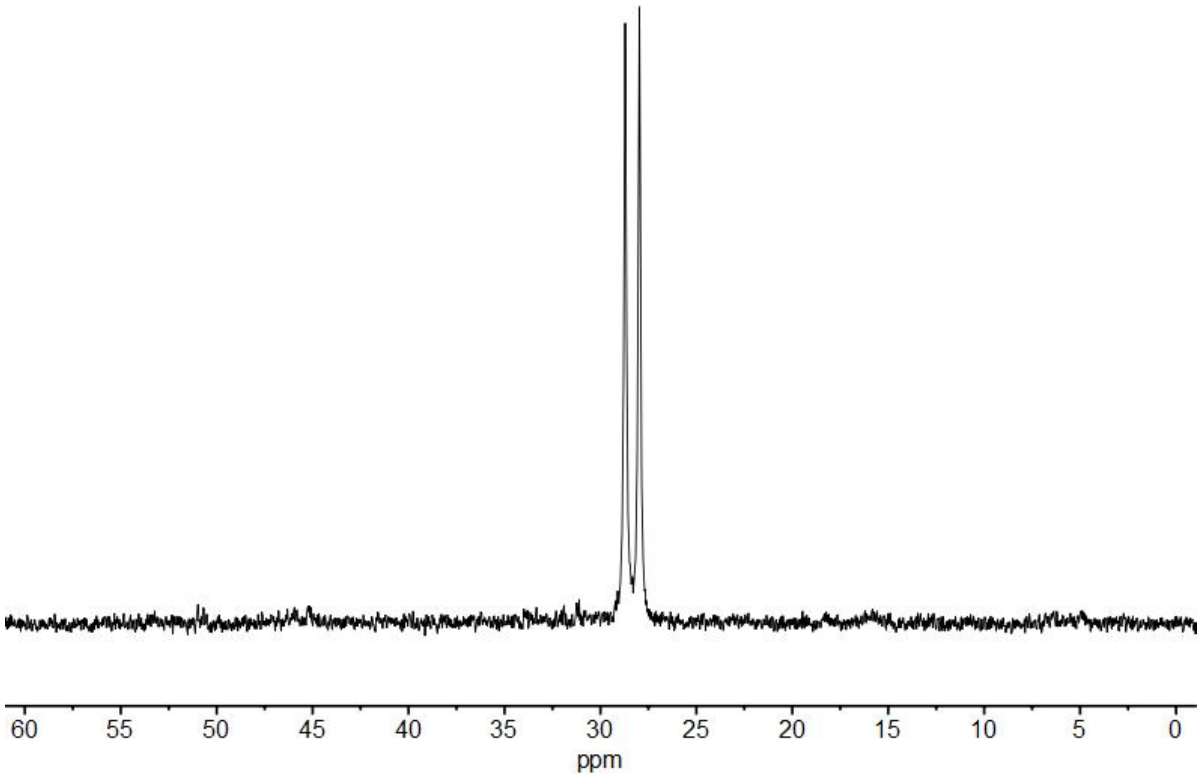

Figure S4. In situ $^{31}P\{^{1}H\}$ NMR spectrum (1,2–$F_2C_6H_4$ solvent, 298 K) of the reaction mixture forming $[Rh_2(DPEphos)_2(\mu\text{–}H)(\mu\text{–}H_2B{=}NHMe)][BAr^F{}_4]$ (**3a**).

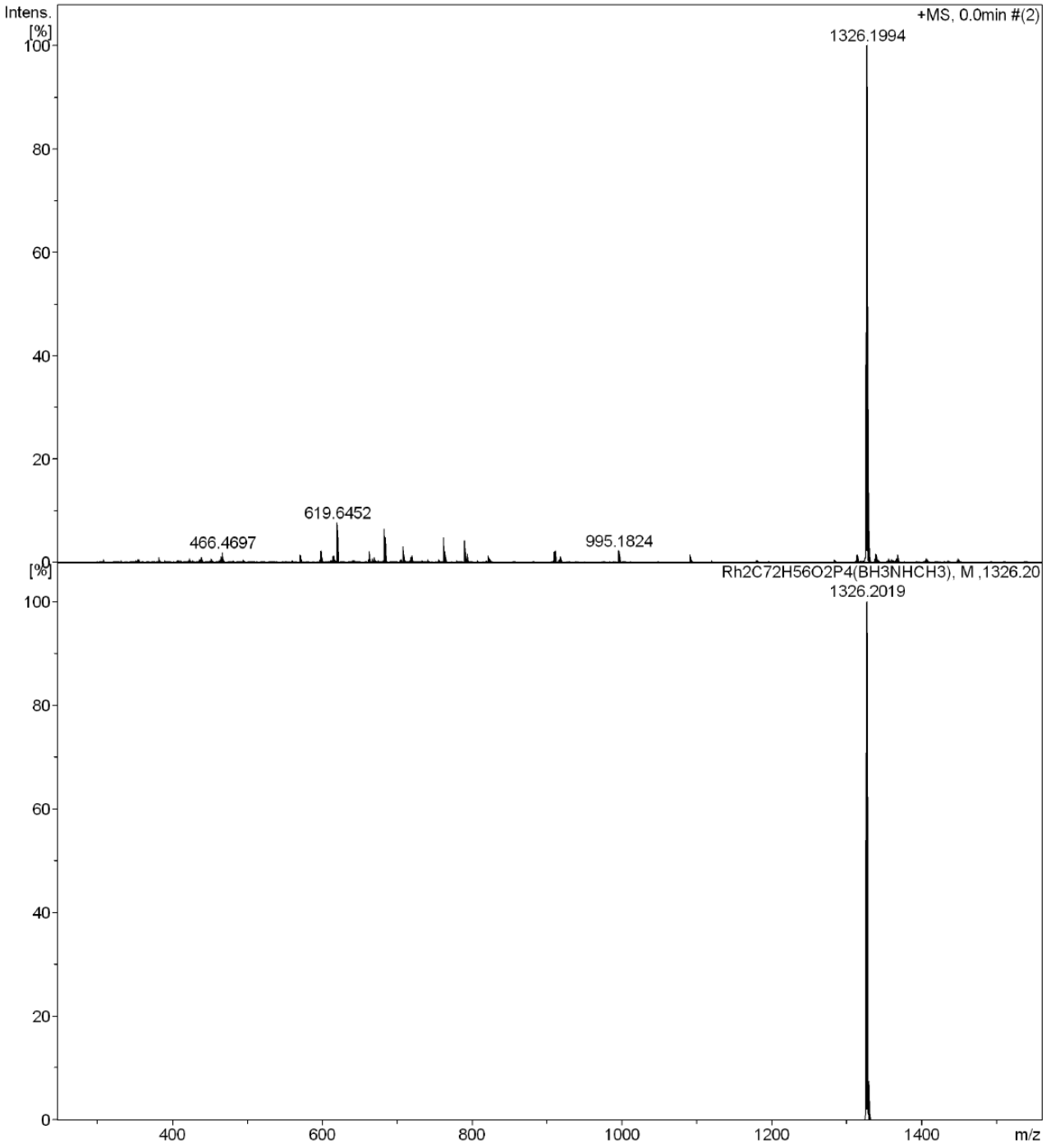

Figure S5. Full experimental (top) and simulated (bottom) ESI mass spectra of the reaction mixture forming $[Rh_2(DPEphos)_2(\mu\text{–}H)(\mu\text{–}H_2B{=}NHMe)][BAr^F{}_4]$ (**3a**).

*Synthesis of [Rh$_2$(DPEphos)$_2$(σ,μ–(H$_2$B)$_2$NHMe)][BAr$^F_4$] (**4a**)*

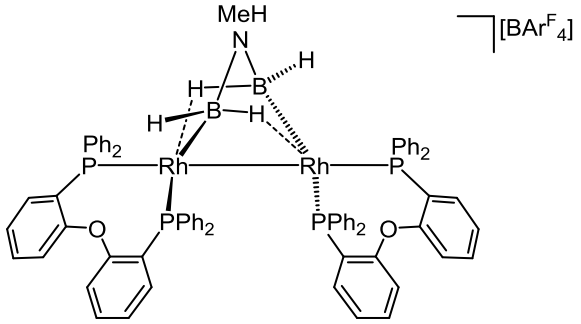

4a

[Rh(DPEphos)(NBD)][BAr$^F_4$] (**1a**) (35.0 mg, 21.9 μmol) and $H_3B{\cdot}NMeH_2$ (4.0 mg, 89.1 μmol) were dissolved in 1,2–$F_2C_6H_4$ (0.4 mL) in a high pressure J. Young NMR tube. The sample was immediately frozen in liquid N_2 and hydrogenated. On warming to room temperature, the mixture was shaken and agitated for 10 minutes, and the light orange solution turned darker in colour. The sample was freeze–pump–thaw degassed three times, backfilled with argon, and agitated for 30 minutes before being placed into the NMR spectrometer. $^{31}P\{^1H\}$ NMR spectroscopy of the fully degassed NMR sample indicated that the mixture subsequently contained 25% [Rh$_2$(DPEphos)$_2$(μ–H)(μ–H$_2$B=NHMe)][BAr$^F_4$] (**3a**) and 75% [Rh$_2$(DPEphos)$_2$(σ,μ–(H$_2$B)$_2$NHMe)][BAr$^F_4$] (**4a**). See Figure S22 for 10 mol% speciation experiment.

Selected spectrometric data: **^{1}H NMR** (400 MHz, 1,2–$F_2C_6H_4$, 298 K): δ −8.41 (d, br, $^2J_{PH}$ 76, Rh$_2$(μ–BH)), −9.25 (m, obscured by **3a** Rh$_2$(μ–BH$_2$) and Rh$_2$(μ–H), Rh$_2$(μ–BH)). Upon decoupling to ^{11}B, the resonance at δ −8.41 sharpened. Upon decoupling to ^{31}P, the resonance at δ −8.41 collapsed to a broad singlet. **^{11}B NMR** (128 MHz, 1,2–$F_2C_6H_4$, 298 K): δ 9.7 (br, Rh(σ,μ–(H$_2$B)$_2$), −6.2 (s, [BAr$^F_4$]$^-$). **^{31}P{^{1}H} NMR** (162 MHz, 1,2–$F_2C_6H_4$, 298 K): δ 31.7 (dd, 1 P, $^1J_{RhP}$ 163, $^2J_{PP}$ 23), 28.9 (dd, 1 P, $^1J_{RhP}$ 159, $^2J_{PP}$ 21), 15.7 (ddd, 1 P, $^1J_{RhP}$ 138, $^2J_{RhP}$ 103, $^2J_{PP}$ 23), 12.8 (ddd, 1 P, $^1J_{RhP}$ 136, $^2J_{RhP}$ 103, $^2J_{PP}$ 21).

*Synthesis of [Rh$_2$(DPEphos)$_2$(σ,μ–(H$_2$B)$_2$NHMe)][Al(OC(CF$_3$)$_3$)$_4$] (**4b**)*

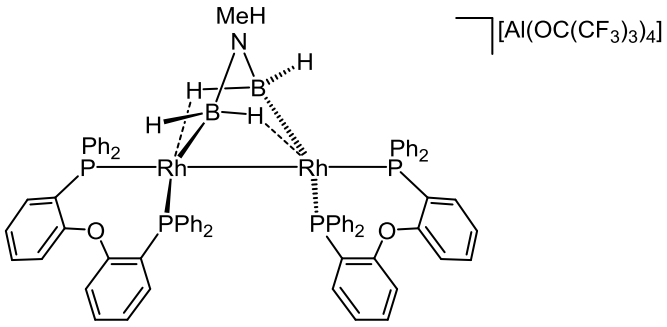

4b

[Rh(DPEphos)(NBD)][Al(OC(CF$_3$)$_3$)$_4$] (**1b**) (40.4 mg, 23.8 μmol) and $H_3B{\cdot}NMeH_2$ (4.2 mg, 93.6 μmol) were dissolved in 1,2–$F_2C_6H_4$ (0.4 mL) in a high pressure J. Young NMR tube. The sample was immediately frozen in liquid N_2 and hydrogenated. On warming to room temperature, the mixture was shaken and agitated for 10 minutes, and the light orange solution turned darker in colour. The sample was freeze–pump–thaw degassed three

times, backfilled with argon, and agitated for 30 minutes before being filtered into a J. Young crystallization flask. The solution was layered with pentane (20.0 mL) at room temperature to yield orange crystals suitable for single crystal X–ray diffraction. The bulk solid of **4b** was analysed by NMR spectroscopy which showed that approximately 5% $[Rh_2(DPEphos)_2(\mu\text{–}H)(\mu\text{–}H_2B{=}NHMe)][Al(OC(CF_3)_3)_4]$ (**3b**) was present by $^{31}P\{^1H\}$ spectroscopy, and dehydrocoupling products of $H_3B{\cdot}NMeH_2$ were also identified by ^{11}B NMR spectroscopy. Yield: 18.0 mg (ca. 7.8 μmol, 66%). See Figure S22 for 10 mol% speciation experiment.

Selected spectrometric data: **^{1}H NMR** (400 MHz, CD_2Cl_2, 298 K): δ 8.06 – 5.78 (m, 54 H, aryl CH), 4.64 (br, 2 H, BH), 3.94 (br, 2 H, aryl CH···Rh), 1.70 (d, 3 H, $^3J_{HH}$ 6, NMe), −8.65 (br, 1 H, $Rh_2(\mu\text{–}HB)$), −9.44 (br, 1 H, $Rh_2(\mu\text{–}HB)$. Upon decoupling to ^{11}B, the resonance at δ 4.64 sharpened, and the resonances at δ −8.65 and −9.44 each sharpened into doublets, revealing $^2J_{PH}$ coupling constants of 73.9 and 68.8, respectively. Upon decoupling to ^{31}P, the resonances at δ −8.65 and −9.44 each collapsed to broad singlets. **^{11}B NMR** (128 MHz, CD_2Cl_2, 298 K): δ 9.4 (br, $Rh(\sigma,\mu\text{–}(H_2B)_2)$). **^{31}P{^{1}H} NMR** (162 MHz, CD_2Cl_2, 298 K): δ 31.7 (dd, 1 P, $^1J_{RhP}$ 163, $^2J_{PP}$ 23), 28.8 (dd, 1 P, $^1J_{RhP}$ 158, $^2J_{PP}$ 21), 15.7 (ddd, 1 P, $^1J_{RhP}$ 138, $^2J_{RhP}$ 102, $^2J_{PP}$ 23), 13.0 (ddd, 1 P, $^1J_{RhP}$ 135, $^3J_{RhP}$ 102, $^2J_{PP}$ 21). **ESI–MS** (1,2–$F_2C_6H_4$, 60˚C, 4.5 kV): *m/z* 1338.33 (calculated 1338.22 for the $[Rh_2(DPEphos)_2(\sigma,\mu\text{–}(H_2B)_2NHMe)]^+$ fragment, showing the correct isotope pattern).

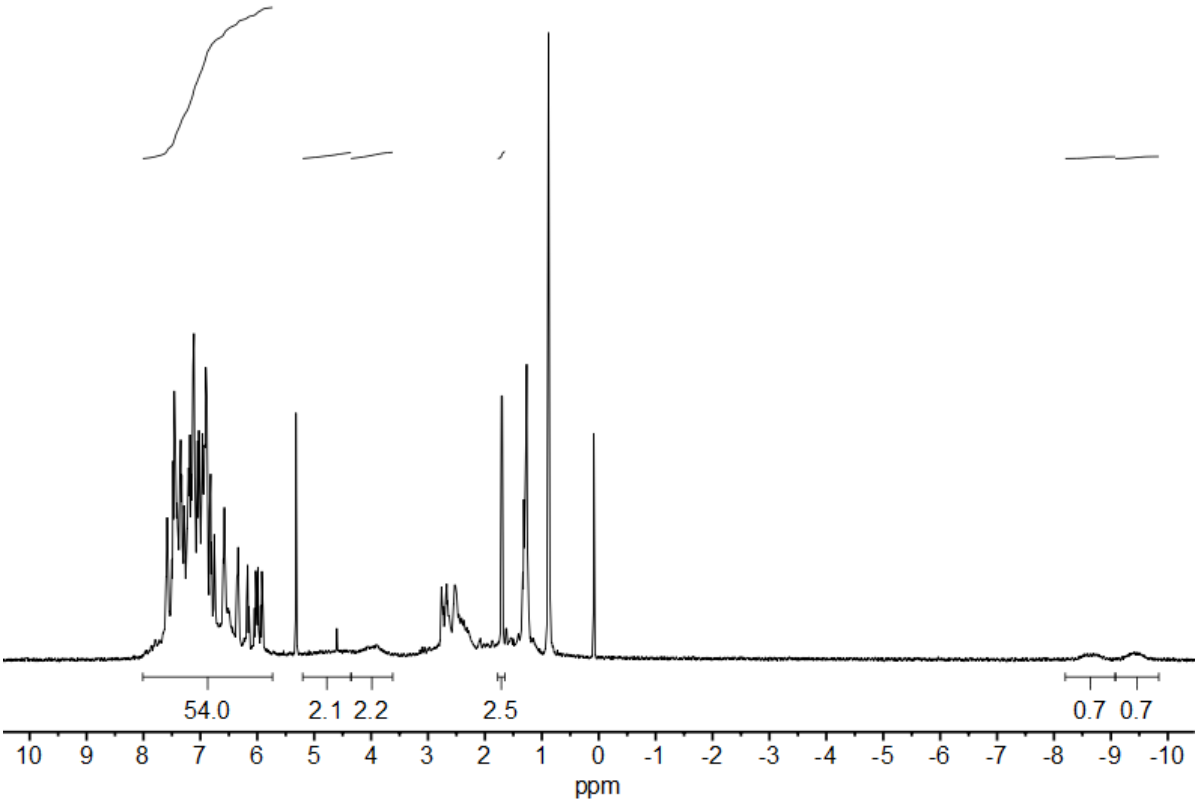

Figure S6. ^{1}H NMR spectrum (CD_2Cl_2 solvent, 298 K) of the bulk material from the crystallization of $[Rh_2(DPEphos)_2(\sigma,\mu\text{–}(H_2B)_2NHMe)][Al(OC(CF_3)_3)_4]$ (**4b**).

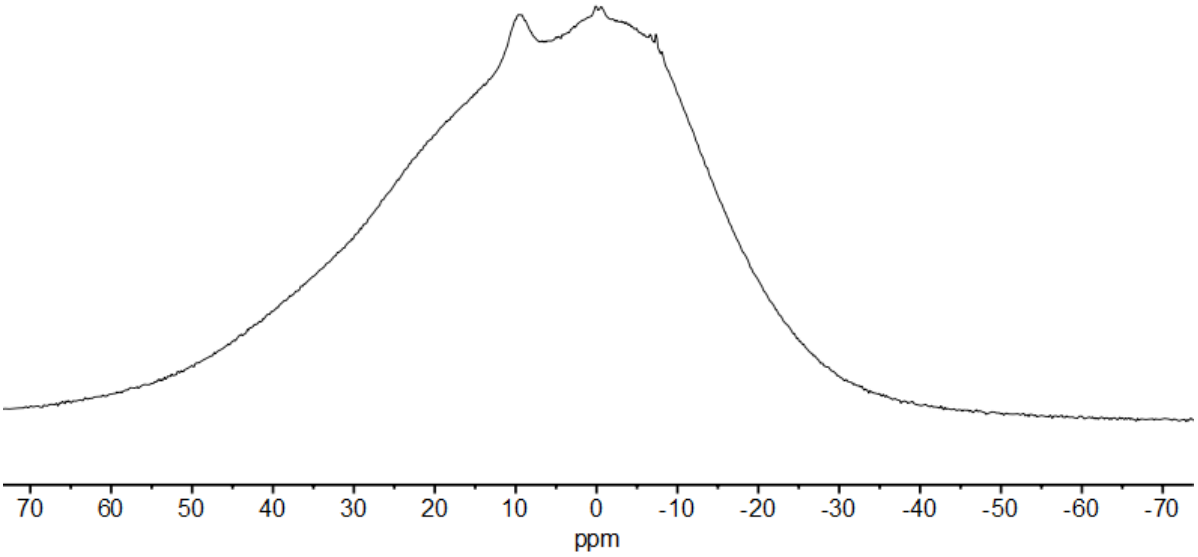

Figure S7. ^{11}B NMR spectrum (CD_2Cl_2 solvent, 298 K) of the bulk material from the crystallization of $[Rh_2(DPEphos)_2(\sigma,\mu\text{–}(H_2B)_2NHMe)][Al(OC(CF_3)_3)_4]$ (**4b**).

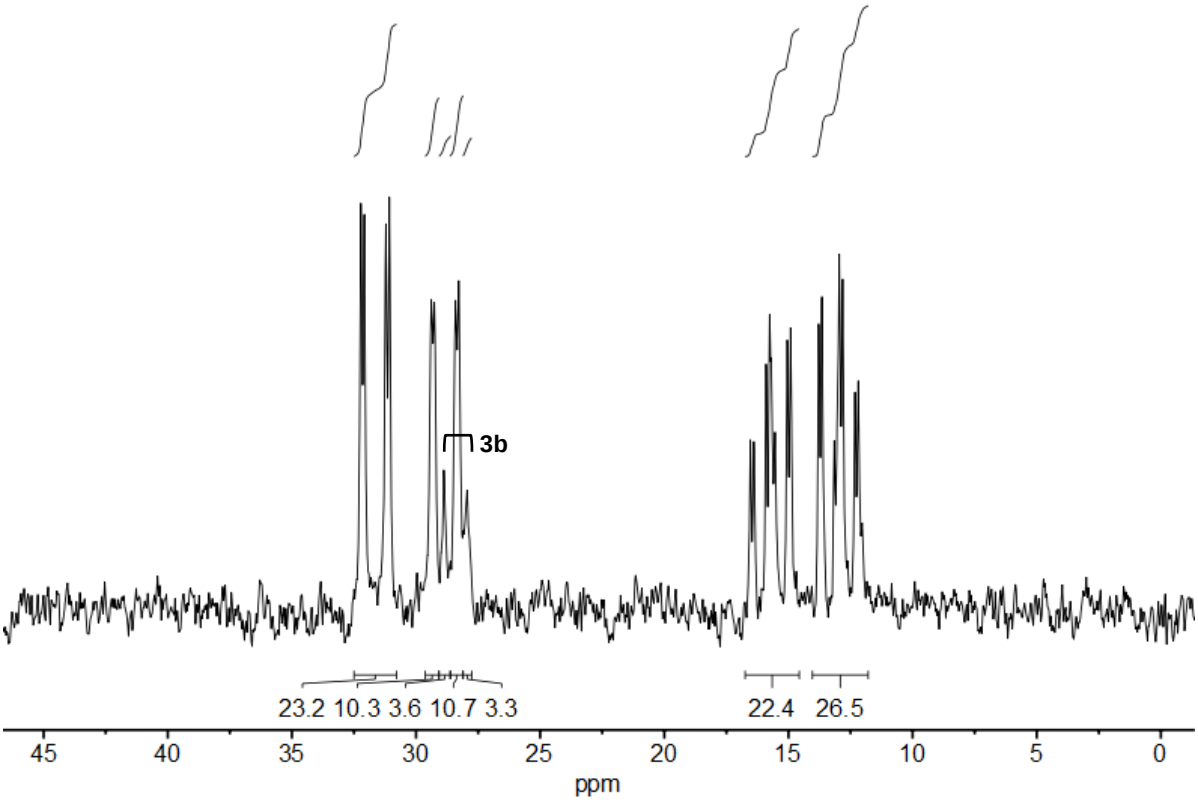

Figure S8. $^{31}P\{^1H\}$ NMR spectrum (CD_2Cl_2 solvent, 298 K) of the bulk material from the crystallization of $[Rh_2(DPEphos)_2(\sigma,\mu\text{–}(H_2B)_2NHMe)][Al(OC(CF_3)_3)_4]$ (**4b**).

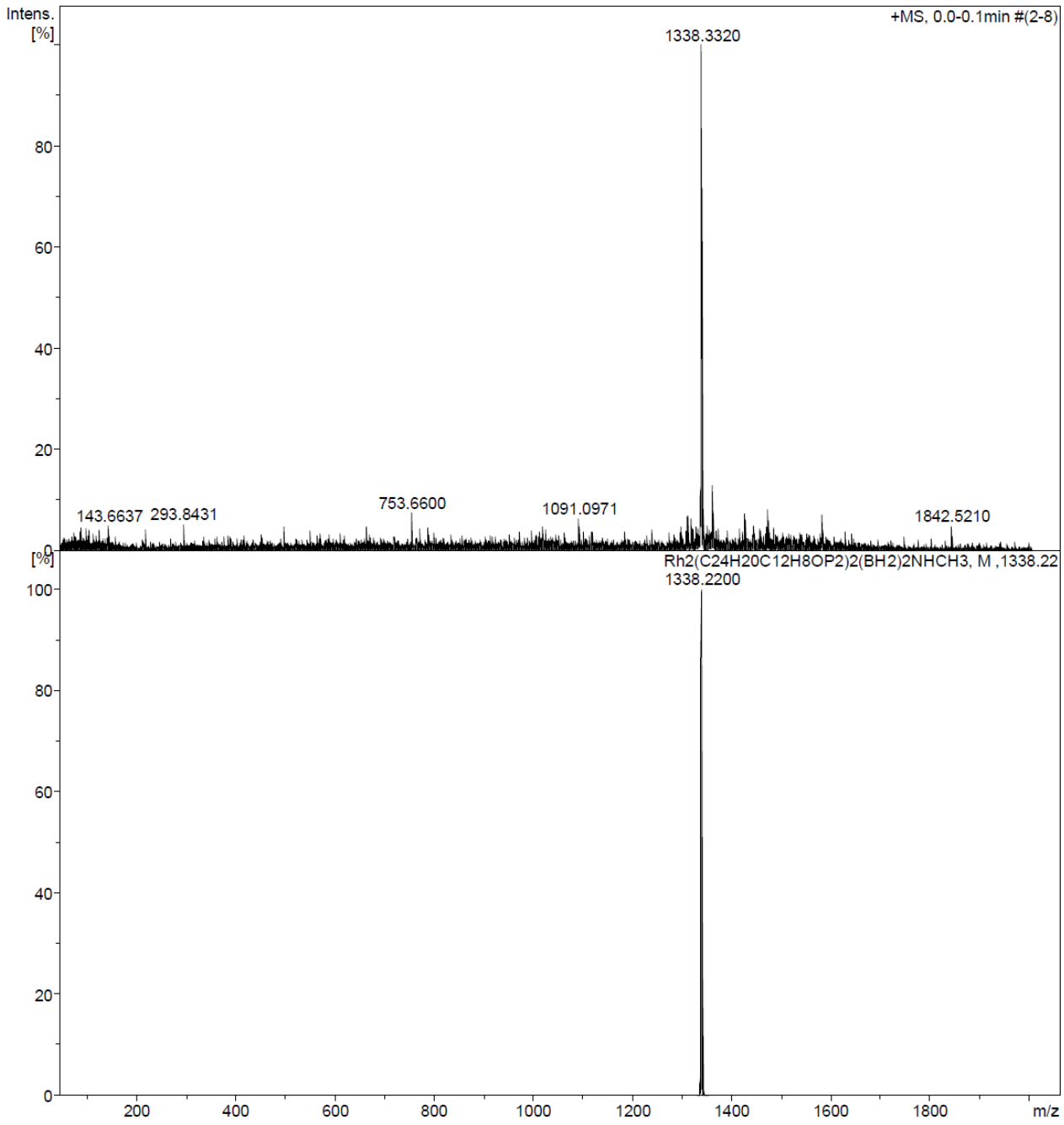

Figure S9. Full experimental (top) and simulated (bottom) ESI mass spectra of the bulk material from the crystallization of $[Rh_2(DPEphos)_2(\sigma,\mu\text{–}(H_2B)_2NHMe)][Al(OC(CF_3)_3)_4]$ (**4b**).

*Synthesis of $[Rh(DPEphos)(H)_2(NMeH_2)_2][BAr^F{}_4]$ (**5**)*

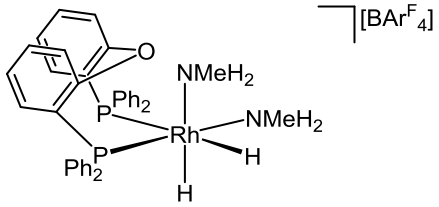

5

Route A: [Rh(DPEphos)(NBD)][BAr^F_4] (**1a**) (17.8 mg, 11.1 μmol) was dissolved in 1,2–$F_2C_6H_4$ (0.25 mL) in a high pressure J. Young NMR tube. 0.25 mL of a 0.0892 M solution of $NMeH_2$ in THF (22.3 μmol) was added. The reaction mixture was immediately frozen in liquid N_2 and hydrogenated. On warming to room temperature, the mixture was shaken, and the light orange solution turned darker in colour. The sample was immediately placed into the NMR spectrometer. $^{31}P\{^1H\}$ NMR spectroscopy indicated that the mixture contained 95% [Rh(DPEphos)$(H)_2(NMeH_2)_2$][BAr^F_4] (**5**) and 5% [Rh(DPEphos)$(NMeH_2)_2$][BAr^F_4] (**6**). Under extended degassing, **5** loses H_2 to form **6**.

Route B: [Rh(DPEphos)(NBD)][BAr^F_4] (**1a**) (35.0 mg, 21.9 μmol) and $H_3B{\cdot}NMeH_2$ (4.0 mg, 89.1 μmol) were dissolved in 1,2–$F_2C_6H_4$ (0.4 mL) in a high pressure J. Young NMR tube. The sample was immediately frozen in liquid N_2 and hydrogenated. On warming to room temperature, the mixture was shaken and agitated for 10 minutes, and the light orange solution turned darker in colour. The sample was freeze–pump–thaw degassed three times and agitated for 30 minutes before being placed into the NMR spectrometer. $^{31}P\{^1H\}$ NMR spectroscopy of the NMR sample indicated that the mixture subsequently contained 25% [Rh_2(DPEphos)$_2$(μ–H)(μ–H_2B=NHMe)][BAr^F_4] (**3a**) and 75% [Rh_2(DPEphos)$_2$(σ,μ–$(H_2B)_2$NHMe)][BAr^F_4] (**4a**). 0.25 mL of a 0.1784 M solution of $NMeH_2$ in THF (44.6 μmol) was added to the sample. $^{31}P\{^1H\}$ NMR spectroscopy of the NMR sample indicated that the mixture contained [Rh(DPEphos)$(H)_2(NMeH_2)_2$][BAr^F_4] (**5**) only, which under extended degassing formed **6**.

Selected spectrometric data: **^{1}H NMR** (400 MHz, 1,2–$F_2C_6H_4$, 298 K): δ −9.61 (dddd, 1 H, $^2J_{PtransH}$ 182, $^2J_{PcisH}$ 24, $^1J_{RhH}$ 18, $^2J_{HH}$ 5, RhH *trans* to P), −16.61 (m, 1 H, RhH *cis* to P). **^{1}H{^{31}P} NMR** (400 MHz, 1,2–$F_2C_6H_4$, 298 K): δ −9.61 (dd, 1 H, $^1J_{RhH}$ 18, $^2J_{HH}$ 5, RhH *trans* to DPEphos–PPh_2), −16.61 (d, br, 1 H, $^1J_{RhH}$ 15, RhH *trans* to $NMeH_2$). **^{31}P{^{1}H} NMR** (162 MHz, 1,2–$F_2C_6H_4$, 298 K): δ 52.2 (d, 1 P, $^1J_{RhP}$ 137), 23.8 (d, br, 1 P, $^1J_{RhP}$ 86).

Route C: [Rh(DPEphos)$(NMeH_2)_2$][BAr^F_4] (**6**) (20.0 mg, 12.8 μmol) was dissolved in CD_2Cl_2 (0.25 mL) in a high pressure J. Young NMR tube. The sample was freeze–pump–thaw degassed three times and hydrogenated, whereupon the orange solution turned slightly darker. The sample was placed in the NMR spectrometer immediately after hydrogenation.

Selected spectrometric data: **^{1}H NMR** (400 MHz, CD_2Cl_2, 298 K): δ 7.72 – 6.10 (m, 49 H, [BAr^F_4]$^-$–CH, aryl CH), 2.32 (m, br, 3 H, NCH_3), 2.12 (m, br, 1 H, NH), 2.09 (t, 3 H, N′CH_3), 1.87 (m, br, 1 H, N′H), 1.72 (m, br, 1 H, N′H), 1.46 (m, br, 1 H, NH), −9.76 (dddd, 1 H, $^2J_{PtransH}$ 180, $^2J_{PcisH}$ 26, $^1J_{RhH}$ 18, $^2J_{HH}$ 5, RhH *trans* to P), −16.78 (m, 1 H, RhH *cis* to P). **^{31}P{^{1}H} NMR** (162 MHz, CD_2Cl_2, 298 K): δ 52.1 (d, 1 P, $^1J_{RhP}$ 137), 24.2 (br, 1 P, $^1J_{RhP}$ 86). **^{1}H NMR** (400 MHz, 1,2–$F_2C_6H_4$, 298 K): δ 8.29 (s, br, 8 H, [BAr^F_4]$^-$–ortho–CH), 7.66 (s, br, 4 H, [BAr^F_4]$^-$–para–CH), 2.23 (m, br, 4 H, overlapping NCH_3, NH), 2.13 (m, br, 3 H, N′CH_3), 2.04 (m, br, 1 H, N′H), 1.89 (m, br, 1 H, N′H), 1.58 (m, br, 1 H, NH), −9.61 (dddd, 1 H, $^2J_{PtransH}$ 182, $^2J_{PcisH}$ 24, $^1J_{RhH}$ 18, $^2J_{HH}$ 5, RhH *trans* to P), −16.61 (m, 1 H, RhH *cis* to P). **^{1}H{^{31}P} NMR** (400 MHz, 1,2–$F_2C_6H_4$, 298 K): δ −9.61 (dd, 1 H, $^1J_{RhH}$ 18, $^2J_{HH}$ 5, RhH *trans* to DPEphos–PPh_2), −16.61 (d, br, 1 H, $^1J_{RhH}$ 15, RhH *trans* to $NMeH_2$). **^{31}P{^{1}H} NMR** (162 MHz, 1,2–$F_2C_6H_4$, 298 K): δ 52.2 (d, 1 P, $^1J_{RhP}$ 137), 23.8 (d, br, 1 P, $^1J_{RhP}$ 86).

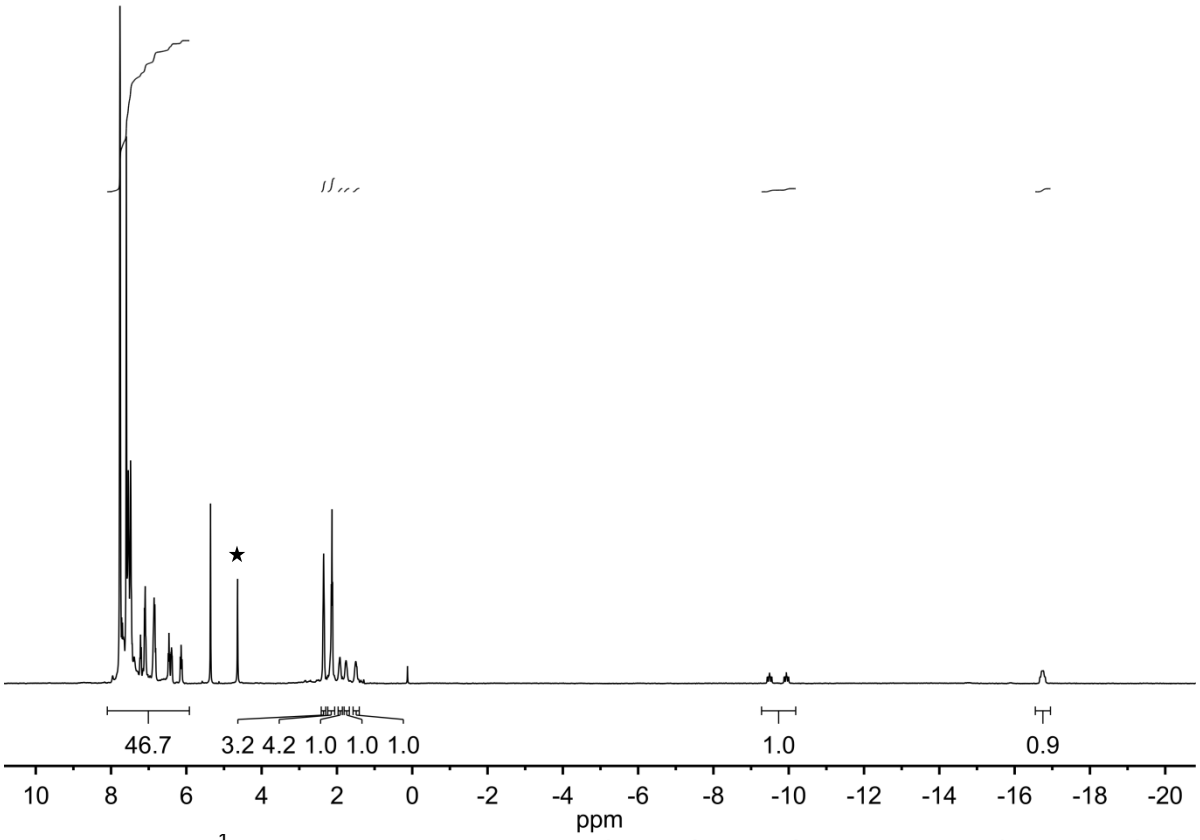

Figure S10. ^{1}H NMR spectrum (CD_2Cl_2 solvent, 298 K) of isolated [Rh(DPEphos)$(H)_2(NMeH_2)_2$][$BAr^F{}_4$] (**5**). The signal marked with a star corresponds to added H_2.

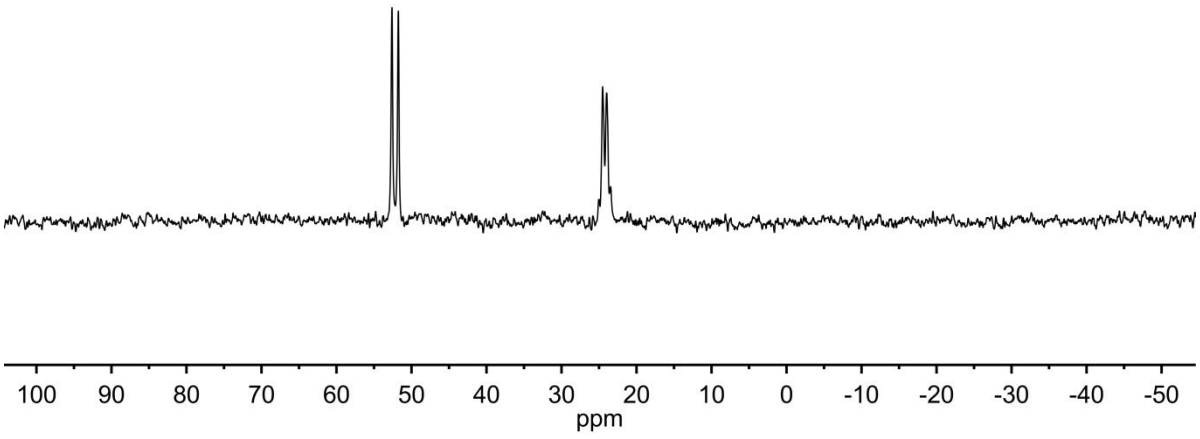

Figure S11. $^{31}P\{^{1}H\}$ NMR spectrum (CD_2Cl_2 solvent, 298 K) of isolated [Rh(DPEphos)$(H)_2(NMeH_2)_2$][$BAr^F{}_4$] (**5**).

*Synthesis of [Rh(DPEphos)(NMeH$_2$)$_2$][BAr$^F{}_4$] (**6**)*

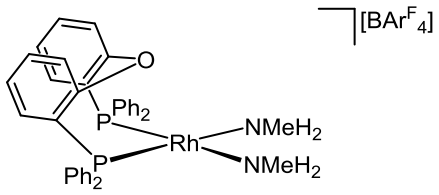

6

Route A: [Rh(DPEphos)(η^2–H$_2$B(NMe$_3$)(CH$_2$)$_2$^{t}Bu)][BAr$^F{}_4$] (**2a**) (18.6 mg, 11.2 μmol) was dissolved in 1,2–F$_2$C$_6$H$_4$ (0.25 mL) in a J. Young NMR tube. 0.25 mL of a 0.0892 M solution of NMeH$_2$ in THF (22.3 μmol) was added. On agitating the sample, the purple solution turned orange in colour. The sample was placed into the NMR spectrometer. ^{31}P{^{1}H} NMR spectroscopy indicated that the mixture contained [Rh(DPEphos)(NMeH$_2$)$_2$][BAr$^F{}_4$] (**6**) as the sole phosphorus–containing species. The sample can be freeze–pump–thaw degassed and hydrogenated, forming **5** as the major organometallic product. Alternatively, the sample containing **6** can be filtered into a J. Young crystallization flask and layered with pentane (20.0 mL) to give an orange oil which was washed with pentane (20.0 mL) and dried under vacuum. Due to the oily nature of this material, bulk material could not be isolated despite repeated attempts.

Route B: To a stirred solution of [Rh(DPEphos)(η^6–o–xylene)][BAr$^F{}_4$] (**7**) (200.0 mg, 124.2 μmol) in 1,2–F$_2$C$_6$H$_4$ (2.0 mL), was added NMeH$_2$ (2.0 M in THF, 0.25 mL, 500 μmol). The resultant orange solution was added dropwise to rapidly stirring pentane (40.0 mL) at −78 °C. The supernatant was decanted and the yellow solid washed with pentane (20 mL × 5) at −78 °C. The sample was subsequently dried in vacuo whilst warming to room temperature (10 minutes). Whilst under vacuum, the resultant oily solid was subjected to repeated freezing in liquid N$_2$ and thawing whilst sonicating (× 5), followed by washing with pentane (10.0 mL × 5), until a yellow powder was obtained. The sample was subsequently dried in vacuo for 1 hour. Yield: 151.6 mg (96.8 μmol, 78%). After extended periods under dynamic vacuum, the compound decomposes. For this reason the sample was more conveniently prepared in situ for kinetics experiments.

Selected spectrometric data: **^{1}H NMR** (400 MHz, CD$_2$Cl$_2$, 298 K): δ 7.72 – 6.71 (m, 49 H, [BAr$^F{}_4$]$^-$–CH, aryl CH), 2.03 (br, 6 H, NCH$_3$), 1.75 (br, 4 H, NH). **^{31}P{^{1}H} NMR** (162 MHz, CD$_2$Cl$_2$, 298 K): δ 39.5 (d, $^1J_{RhP}$ 182). **^{1}H NMR** (400 MHz, 1,2–F$_2$C$_6$H$_4$, 298 K): δ 1.99 (br, 6 H, NCH$_3$), 1.78 (br, 4 H, NH). **^{31}P{^{1}H} NMR** (162 MHz, 1,2–F$_2$C$_6$H$_4$, 298 K): δ 39.7 (d, $^1J_{RhP}$ 180). **ESI–MS** (CH$_2$Cl$_2$, 60˚C, 4.5 kV): The major peak observed by mass spectrometry with *m/z* 669.06 was proposed to be due to formation of the [Rh(DPEphos)(N$_2$)]$^+$ fragment (calculated *m/z* 669.07), showing the correct isotope pattern. This N$_2$ complex can be formed due to the presence of N$_2$ in the flow gas, as has been noted previously.[13]

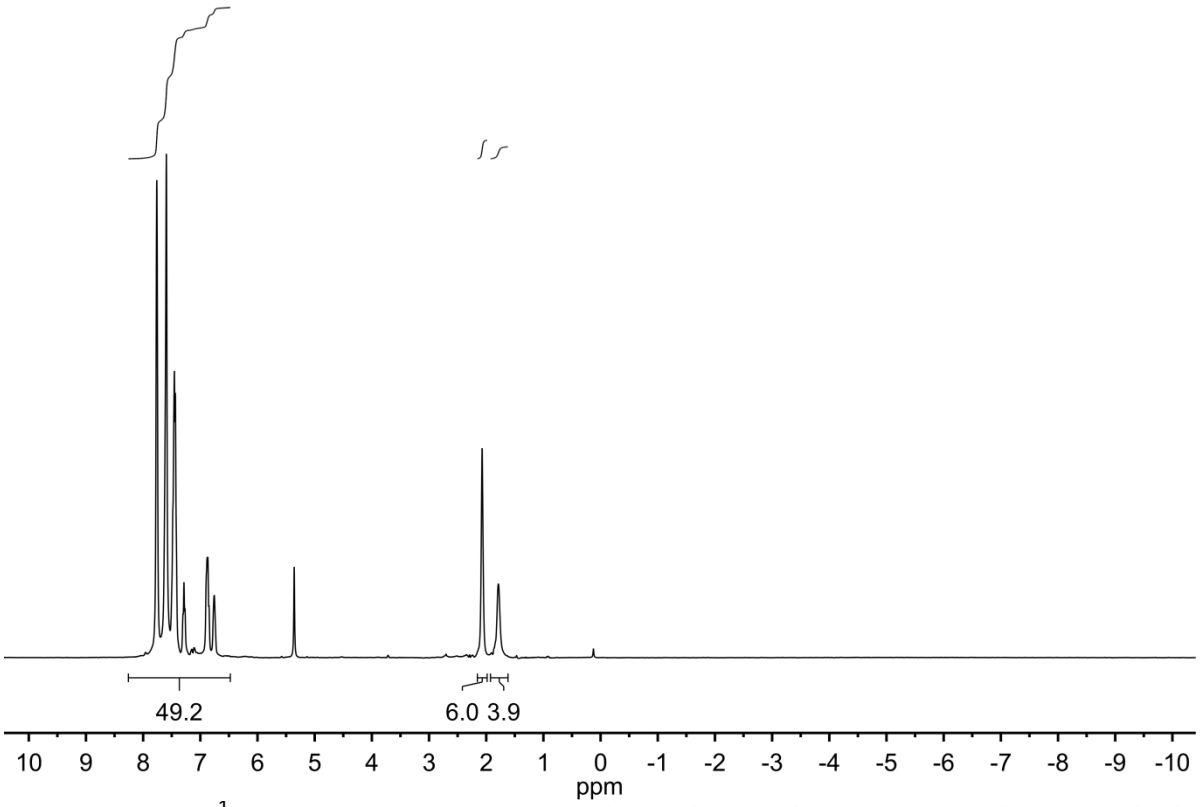

Figure S12. ^{1}H NMR spectrum (CD_2Cl_2 solvent, 298 K) of isolated [Rh(DPEphos)$(NMeH_2)_2$][BAr^F_4] (**6**).

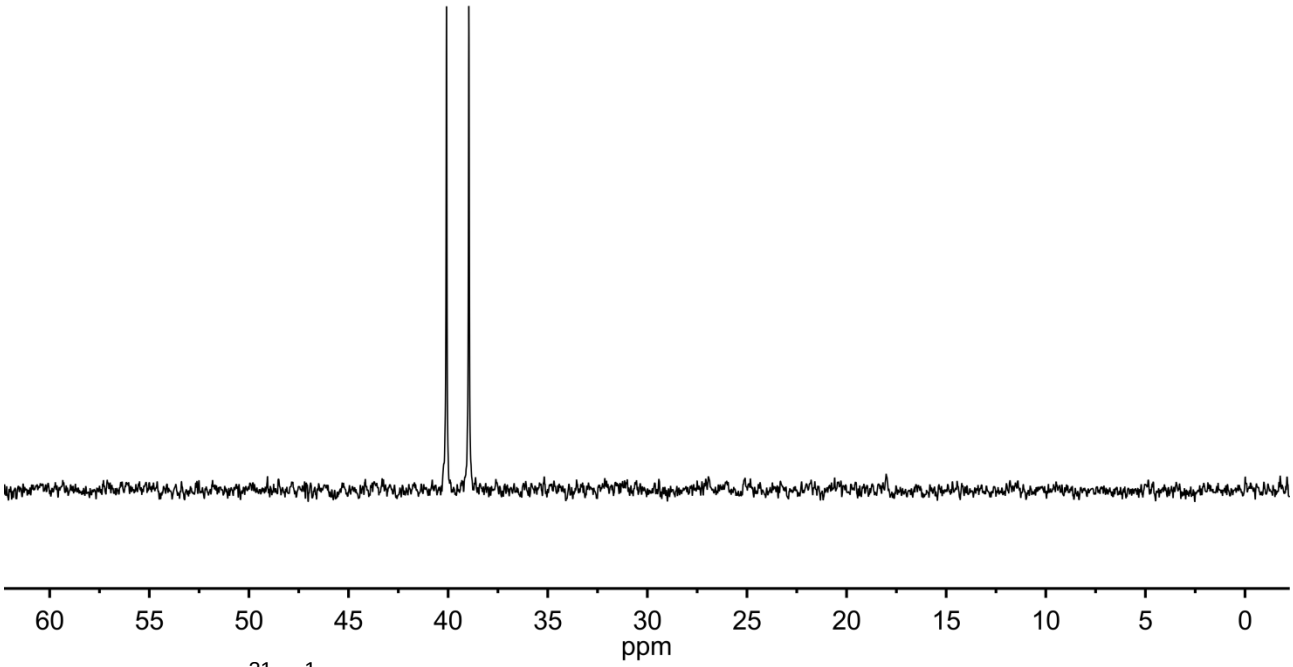

Figure S13. $^{31}P\{^{1}H\}$ NMR spectrum (CD_2Cl_2 solvent, 298 K) of isolated [Rh(DPEphos)$(NMeH_2)_2$][BAr^F_4] (**6**).

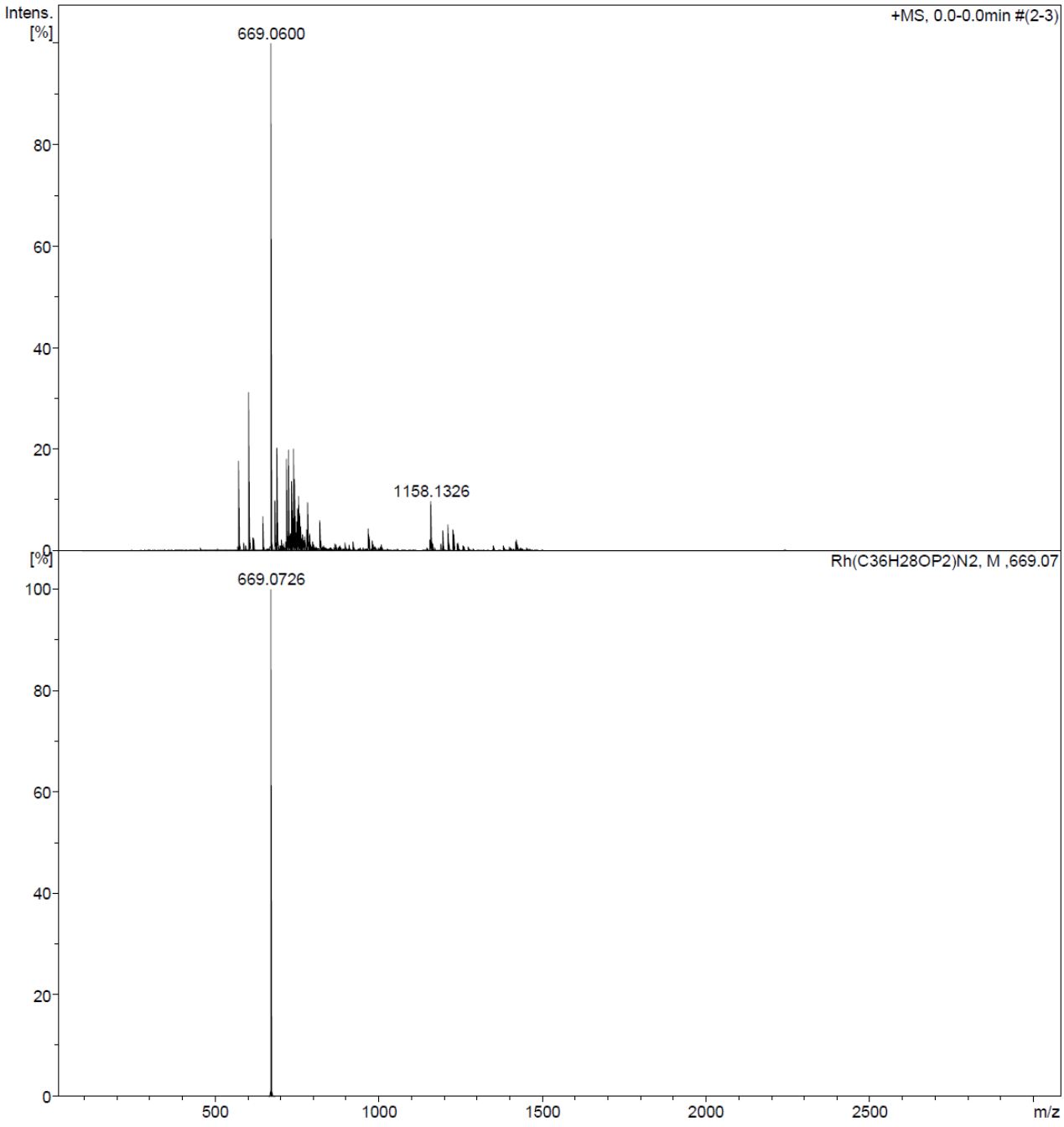

Figure S14. Full experimental ESI mass spectrum (top) of a CH_2Cl_2 solution of $[Rh(DPEphos)(NMeH_2)_2][BAr^F{}_4]$. The major peak is proposed to be due to the $[Rh(DPEphos)(N_2)]^+$ fragment, and the corresponding simulated mass spectrum is shown (bottom).

*Synthesis of [Rh(Xantphos–^{i}Pr)(H)$_2$(NMeH$_2$)][BAr$^{F}_4$] (**8**)*

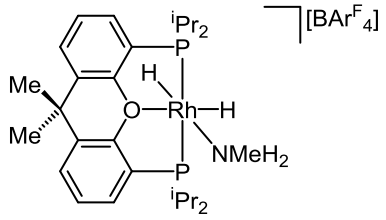

8

Rh(Xantphos–^{i}Pr)(H)$_2$Cl (35.1 mg, 60.0 µmol) and Na[BAr$^{F}_4$] (53.2 mg, 60.0 µmol) were dissolved in 1.0 mL THF in a J. Young crystallisation tube. Immediately, 0.15 mL of a 2.0 M solution of NMeH$_2$ in THF (300.0 µmol) was added. The solution was stirred for 1 hour to give a pale yellow solution and white precipitate. The reaction mixture was filtered and layered with pentane (30.0 mL) and stored at 5˚C, which yielded pale yellow crystals. The crystals were isolated by filtration, washed with pentane (5.0 mL × 3) and dried under vacuum. Yield 53.2 mg (36.9 µmol, 62%).

^{1}H NMR (500 MHz, CD_2Cl_2, 298 K): δ 7.72 (s, br, 8 H, [BAr$^{F}_4$]$^{-}$–ortho–CH), 7.67 (d, 2 H, $^{2}J_{HH}$ 8, aryl CH para to P), 7.56 (s, br, 4 H, [BAr$^{F}_4$]$^{-}$–para–CH), 7.52 (m, 2 H, aryl CH meta to P), 7.42 (dd, 2 H, $^{2}J_{HH}$ 8, $^{2}J_{PH}$ 8, aryl CH ortho to P), 2.62 (br, 2 H, NH), 2.51 (s, br, 4 H, ^{i}Pr–CH), 2.32 (t, 3 H, $^{3}J_{HH}$ 6, NMe), 1.89 (s, 3 H, Xantphos 'backbone' C(CH$_3$)), 1.44 (m, 6 H, ^{i}Pr–CH$_3$), 1.34 (s, 3 H, Xantphos 'backbone' C(CH$_3$)), 1.26 (m, 6 H, ^{i}Pr–CH$_3$), 1.19 (m, 6 H, ^{i}Pr–CH$_3$), 0.75 (m, 6 H, ^{i}Pr–CH$_3$), −17.73 (br, 1 H, RhH), −20.40 (br, 1 H, RhH). **^{31}P{^{1}H} NMR** (202 MHz, CD_2Cl_2, 298 K): δ 64.0 (d, $^{1}J_{RhP}$ 111). **ESI–MS** (1,2–$F_2C_6H_4$, 60˚C, 4.5 kV): *m/z* 547.20 (calculated 547.18 for the [Rh(Xantphos–^{i}Pr)]$^{+}$ fragment, showing the correct isotope pattern). **Elemental Microanalysis**: Calc. ($C_{60}H_{59}B_1F_{24}N_1O_1P_2Rh_1$): C, 49.98; H, 4.12; N, 0.97. Found: C, 49.83; H, 3.97; N, 0.92.

Proposed Synthesis of Tentatively Characterised [Rh$_2$(DPEphos)$_2$(B$_2$H$_5$)][BAr$^{F}_4$]

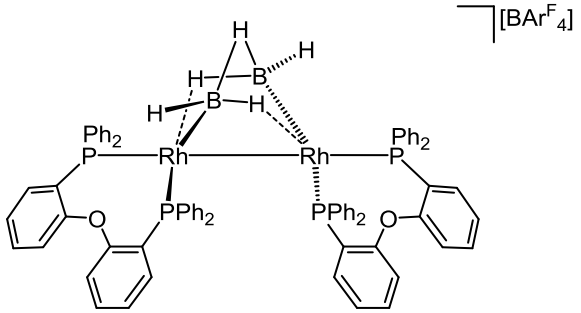

Possible structure of proposed complex
[Rh$_2$(DPEphos)$_2$(B$_2$H$_5$)][BAr$^{F}_4$]

[Rh(DPEphos)(η^{2}–H$_2$B(NMe$_3$)(CH$_2$)$_2$^{t}Bu)][BAr$^{F}_4$] (**2a**) (14.0 mg, 8.4 µmol) was dissolved in THF solvent (0.35 mL) in a J. Young NMR tube. 0.11 mL of a 0.08 M solution of H$_3$B·THF (8.8 µmol) was added. The purple solution turned orange on addition of H$_3$B·THF. The sample was immediately placed into the NMR spectrometer.

Selected spectrometric data: **^{31}P{^{1}H} NMR** (162 MHz, THF, 298 K): δ 32.0 (d, 2 P, $^{1}J_{RhP}$ 151), 17.5 (d, br, 2 P, $^{1}J_{RhP}$ ~120). **ESI−MS** (1,2−$F_2C_6H_4$, 60˚C, 4.5 kV): The major peak observed by mass spectrometry with *m/z* 1309.16 was proposed to be due to formation of a $[\{Rh(DPEphos)\}_2(B_2H_5)]^+$ fragment (calculated *m/z* 1309.19), showing the correct isotope pattern. There are also minor peaks observed at *m/z* 1321.18 and *m/z* 1335.21, proposed to be due to the formation of the borane−derived fragments $[\{Rh(DPEphos)\}_2(B_3H_6)]^+$ (calculated *m/z* 1321.21) and $[\{Rh(DPEphos)\}_2(B_4H_9)]^+$ (calculated *m/z* 1335.25) with the correct isotope patterns, respectively.

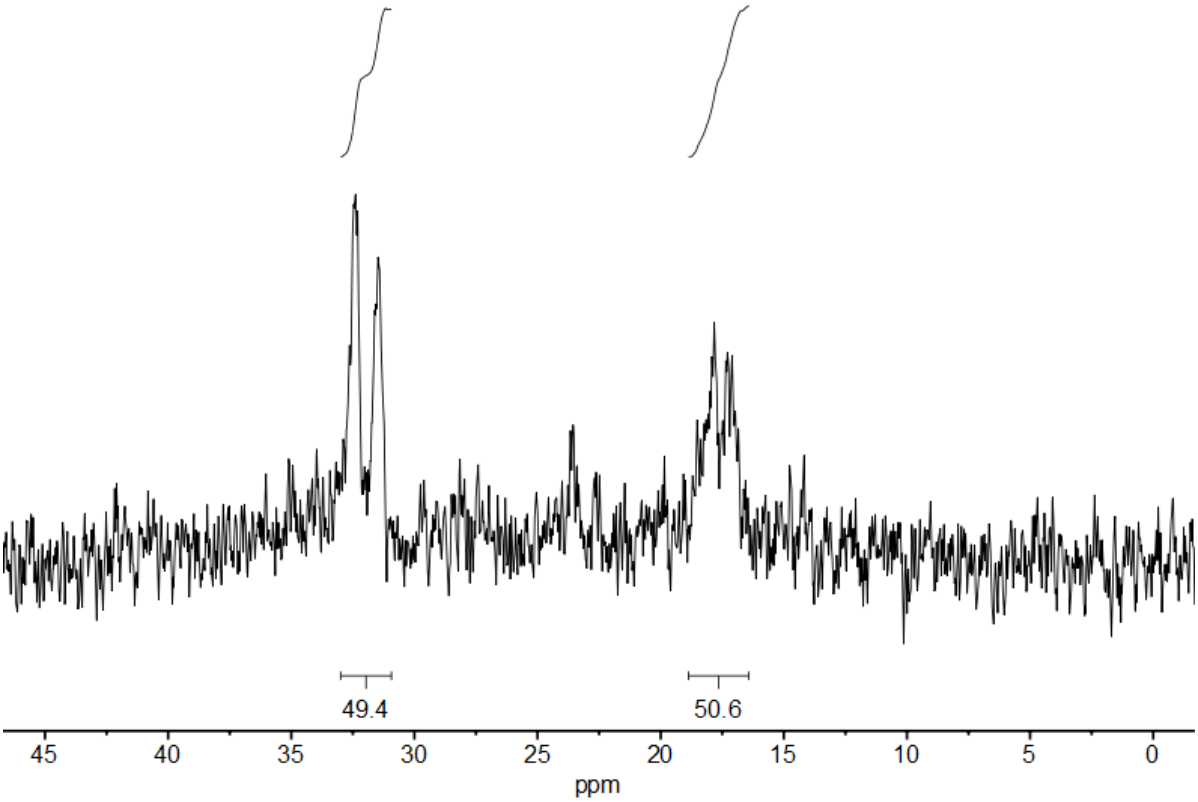

Figure S15. In situ $^{31}P\{^{1}H\}$ NMR spectrum (THF solvent, 298 K) of the reaction mixture of $[Rh(DPEphos)(\eta^2\text{–}H_2B(NMe_3)(CH_2)_2{}^tBu)][BAr^F{}_4]$ (**2a**) and 1 equiv. $H_3B{\cdot}THF$ in THF solvent, forming proposed $[Rh_2(DPEphos)_2(B_2H_5)][BAr^F{}_4]$.

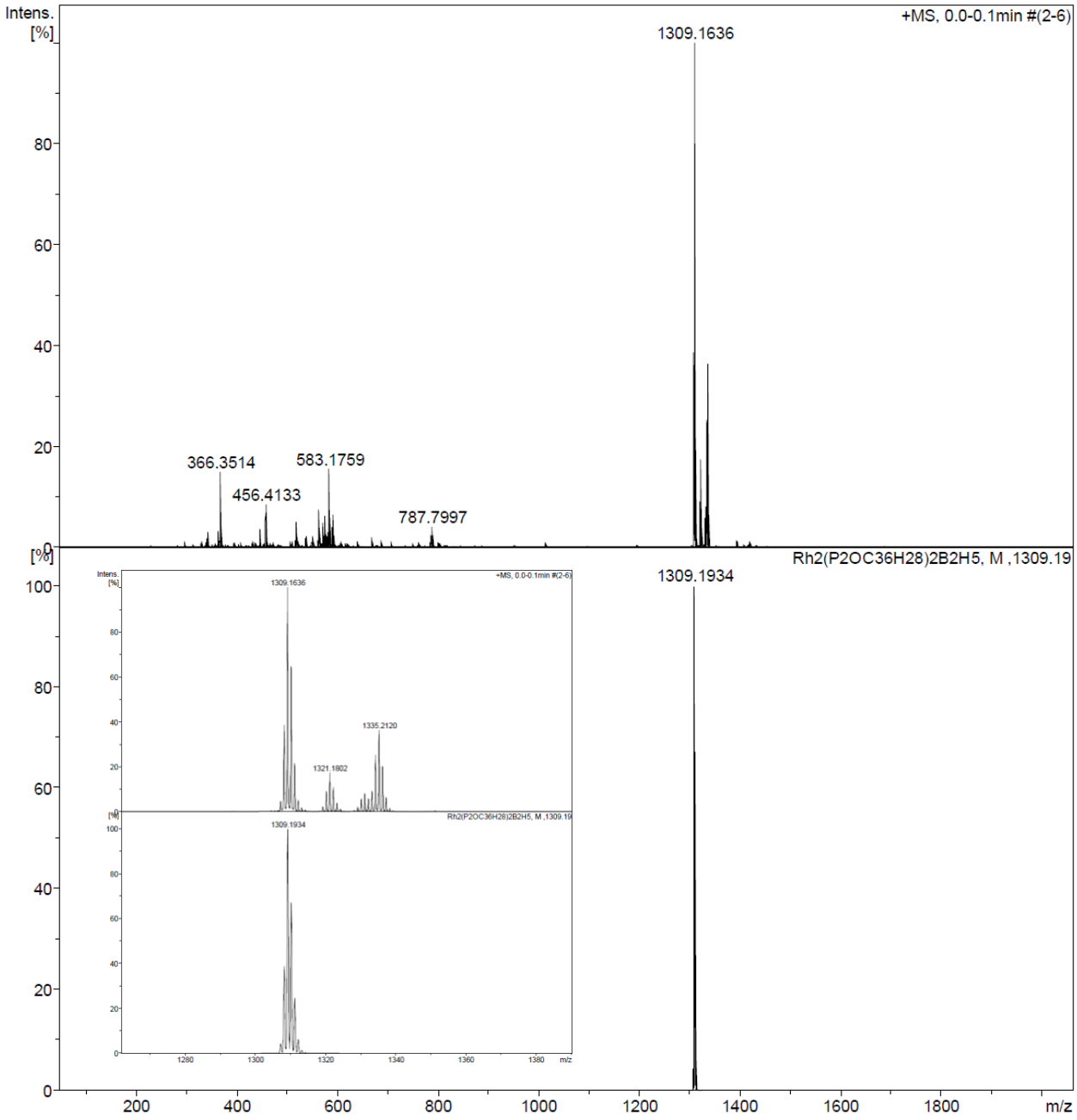

Figure S16. Full experimental (top) and simulated (bottom) ESI mass spectra of the reaction mixture forming the proposed borane−derived species $[Rh_2(DPEphos)_2(B_2H_5)][BAr^F{}_4]$. Inset: Zoom-in showing the isotope pattern: experimental (top) and simulated (bottom).

Catalytic Dehydropolymerization of $H_3B{\cdot}NMeH_2$

Dehydropolymerization Under Open Conditions

In a typical experiment (e.g. 0.223 M $[H_3B{\cdot}NMeH_2]$, 0.2 mol% catalyst loading), $H_3B{\cdot}NMeH_2$ (50.0 mg, 1110.0 µmol) was suspended in 4.5 mL 1,2–$F_2C_6H_4$ in a two–neck Schlenk flask. Double the desired amount of the catalyst was weighed into a separate flask and dissolved in 1.0 mL 1,2–$F_2C_6H_4$. The $H_3B{\cdot}NMeH_2$–containing flask was connected to an external mineral oil bubbler and the argon flow was controlled to achieve

a rate of bubbling of approximately 2 bubbles s^{-1}. 0.5 mL of the catalyst solution was added to the reaction mixture and the resultant solution was stirred for the desired reaction time at 400 rpm. 0.3 mL of the reaction mixture was removed for analysis by NMR spectroscopy. The remaining reaction mixture was decanted into 40.0 mL of rapidly stirring hexane to give an off–white suspension which was stirred for 5 minutes to allow polymer precipitation, then isolated by filtration. The off–white solid $(H_2BNMeH)_n$ was dried under vacuum overnight. Isolated yields of $(H_2BNMeH)_n$ varied from 30% to 65%.

Dehydropolymerization Under Hydrogen Evolution Measurement Conditions

In a typical experiment (e.g. 0.223 M [$H_3B{\cdot}NMeH_2$], 0.2 mol% catalyst loading), $H_3B{\cdot}NMeH_2$ (50.0 mg, 1110.0 µmol) was suspended in 4.5 mL 1,2–$F_2C_6H_4$ in a jacketed two–neck Schlenk flask connected to a recirculating cooler and the temperature set at 20°C. Double the desired amount of the catalyst was weighed into a separate flask and dissolved in 1.0 mL 1,2–$F_2C_6H_4$. The $H_3B{\cdot}NMeH_2$–containing flask was sealed off from the argon supply and connected to a water–filled 100.0 mL gas burette. 0.5 mL of the catalyst solution was added to the reaction mixture and the resultant solution was stirred at 400 rpm. The time taken per 1.0 mL of gas to evolve was recorded. Upon completion of gas evolution, 0.3 mL of the reaction mixture was removed for analysis by NMR spectroscopy. The remaining reaction mixture was decanted into 40.0 mL of rapidly stirring hexane to give an off–white suspension which was stirred for 5 minutes to allow polymer precipitation, then isolated by filtration. The off–white solid $(H_2BNMeH)_n$ was dried under vacuum overnight. Isolated yields of $(H_2BNMeH)_n$ varied from 30% to 60%.

Dehydropolymerization Under Closed Conditions

In a typical experiment (e.g. 0.223 M [$H_3B{\cdot}NMeH_2$], 0.2 mol% catalyst loading), $H_3B{\cdot}NMeH_2$ (50.0 mg, 1110.0 µmol) was suspended in 4.5 mL 1,2–$F_2C_6H_4$ in a J. Young flask. Double the desired amount of the catalyst was weighed into a separate flask and dissolved in 1.0 mL 1,2–$F_2C_6H_4$. 0.5 mL of the catalyst solution was added to the reaction mixture and the flask was sealed and stirred for the desired reaction time at 400 rpm. 0.3 mL of the reaction mixture was removed for analysis by NMR spectroscopy. The remaining reaction mixture was decanted into 40.0 mL of rapidly stirring hexane to give an off–white suspension which was stirred for 5 minutes to allow polymer precipitation, then isolated by filtration. The off–white solid $(H_2BNMeH)_n$ was dried under vacuum overnight. Isolated yields of $(H_2BNMeH)_n$ varied from 20% to 45%.

Dehydropolymerization Recharging Experiments

Dehydropolymerization was conducted as per standard gas evolution measurement conditions. After cessation of gas evolution, the reaction mixture was transferred by syringe into a second jacketed, two–neck Schlenk flask connected to a recirculating cooler at 20°C containing $H_3B{\cdot}NMeH_2$ (50.0 mg, 1110 µmol). Gas evolution was recorded by gas burette. After cessation of gas evolution, the reaction mixture was transferred by syringe into a third jacketed, two–neck Schlenk flask connected to a recirculating cooler at 20°C containing $H_3B{\cdot}NMeH_2$ (50.0 mg, 1110 µmol). Gas evolution was recorded by gas burette. After cessation of gas evolution, 0.3 mL of the reaction mixture was removed for analysis by NMR spectroscopy. The remaining reaction mixture was decanted into 40.0 mL of rapidly stirring hexane, stirred for 5 minutes to allow polymer precipitation, then isolated by filtration. The off–white solid $(H_2BNMeH)_n$ was dried under vacuum overnight. Isolated yield of $(H_2BNMeH)_n$ 80.0 mg (53%).

Molecular Weight vs Conversion Procedure

For molecular weight vs conversion experiments, the general dehydropolymerization procedure was followed. At various time points, PPh_3 (5 equivs. relative to Rh via 0.2 mL 1,2−$F_2C_6H_4$) was added to stop catalysis. Hexane (30 mL) was added to the reaction flask and the precipitate was isolated by filtration and dried under vacuum for 30 minutes. A sample was dissolved in protio−THF and analyzed by ^{11}B NMR spectroscopy to determine the % conversion calculated by integration of the relevant signals. Polymer samples were dried overnight prior to GPC analysis.

Tests for Catalyst Homogeneity: Mercury Poisoning

Dehydropolymerization was conducted as per standard gas evolution measurement conditions. After a short time, an excess of elemental mercury (ca. 0.05 mL) was added. No inhibition of gas evolution was observed, consistent with homogeneous catalysis.

Tests for Catalyst Homogeneity: PPh_3 Fractional Poisoning

Dehydropolymerization was conducted as per standard gas evolution measurement conditions. After a short time, 0.2 equivs. (relative to catalyst) of PPh_3 in 0.2 mL 1,2–$F_2C_6H_4$ was added. A minor decrease in the rate of gas evolution was observed, consistent with homogeneous catalysis.

Dehydropolymerization under THF, BH_3 or $NMeH_2$–doped conditions

$H_3B{\cdot}NMeH_2$ (50.0 mg, 1110.0 µmol) was suspended in 4.45 mL 1,2–$F_2C_6H_4$ in a jacketed two–neck Schlenk flask connected to a recirculating cooler and the temperature set at 20°C. Double the desired amount of the catalyst was weighed into a separate flask and dissolved in 1.0 mL 1,2–$F_2C_6H_4$. The $H_3B{\cdot}NMeH_2$–containing flask was sealed off from the argon supply and connected to a water–filled 100.0 mL gas burette. 0.5 mL of the catalyst solution was added to the reaction mixture and the resultant solution was stirred at 400 rpm. After 5 seconds, the desired number of equivalents (relative to catalyst) of the desired doping agent in 0.05 mL (50 µL) THF was added. For example, for ~1 equiv. BH_3 at 0.4 mol% **2a**, 0.05 mL (50 µL) of a 0.0892 M solution of $BH_3{\cdot}THF$ was added. The time taken per 1.0 mL of gas to evolve was recorded. Upon completion of gas evolution, 0.3 mL of the reaction mixture was removed for analysis by NMR spectroscopy. The remaining reaction mixture was decanted into 40.0 mL of rapidly stirring hexane to give an off–white suspension which was stirred for 5 minutes to allow polymer precipitation, then isolated by filtration. The off–white solid $(H_2BNMeH)_n$ was dried under vacuum overnight. Isolated yields of $(H_2BNMeH)_n$ varied from 25% to 50%.

*In Situ Preparation of **3a** as a Catalyst for $H_3B{\cdot}NMeH_2$ Dehydropolymerization*

[Rh(DPEphos)(NBD)][$BAr^F{}_4$] (**1a**) (35.0 mg, 21.9 µmol) and $H_3B{\cdot}NMeH_2$ (2.0 mg, 44.6 µmol) were dissolved in 1,2–$F_2C_6H_4$ (2.5 mL) in a J. Young flask. The sample was immediately frozen in liquid N_2 and hydrogenated. On warming to room temperature, the mixture was stirred for 10 minutes, and the light orange solution turned darker in colour. 0.5 mL of this solution was removed for analysis by $^{31}P\{^1H\}$ NMR spectroscopy, which showed that the sole phosphorus–containing species was complex **3a**. A further 0.5 mL of the solution containing 2.2 µmol **3a** (4.4 µmol relative to Rh_{TOTAL}) was removed via syringe and used as a catalyst for $H_3B{\cdot}NMeH_2$ dehydropolymerization under hydrogen evolution

measurements conditions as per the general procedure (vide supra), at 0.2 mol% catalyst loading of **3a** (0.4 mol% with respect to Rh_{TOTAL}).

*In Situ Preparation of **5/6** as a Catalyst for $H_3B{\cdot}NMeH_2$ Dehydropolymerization*

The desired amount of [Rh(DPEphos)(NBD)][BAr^F_4] (**1a**) was dissolved in the desired volume of 1,2–$F_2C_6H_4$ solvent in a J. Young flask. ~2 equivs. relative to catalyst of $NMeH_2$ in THF was added. The objective was to add 0.5 mL of the desired amount of in situ formed **5**/**6**, of which 0.45 mL was 1,2–$F_2C_6H_4$ solvent and 0.05 mL was THF solvent, to allow direct comparison between catalyst loadings. For 0.2 mol% catalyst loading of **5**/**6**, [Rh(DPEphos)(NBD)][BAr^F_4] (**1a**) (17.8 mg, 11.1 µmol) was dissolved in 1,2–$F_2C_6H_4$ (2.25 mL) in a J. Young flask. 0.25 mL of a 0.0892 M solution of $NMeH_2$ in THF (22.3 µmol) was added, giving a 2.5 mL solution. For 0.4 mol% catalyst loading of **5**/**6**, [Rh(DPEphos)(NBD)][BAr^F_4] (**1a**) (35.6 mg, 22.3 µmol) was dissolved in 1,2–$F_2C_6H_4$ (2.25 mL) in a J. Young flask. 0.25 mL of a 0.1784 M solution of $NMeH_2$ in THF (44.6 µmol) was added, giving a 2.5 mL solution. For 1.0 mol% catalyst loading of **5**/**6**, [Rh(DPEphos)(NBD)][BAr^F_4] (**1a**) (35.6 mg, 22.3 µmol) was dissolved in 1,2–$F_2C_6H_4$ (0.9 mL) in a J. Young flask. 0.1 mL of a 0.4460 M solution of $NMeH_2$ in THF (44.6 µmol) was added, giving a 1.0 mL solution. In all cases, the reaction mixtures were immediately frozen in liquid N_2 and hydrogenated. On warming to room temperature, the mixtures were shaken, and the light orange solutions turned darker in colour. The reaction mixtures were freeze–pump–thaw degassed three times and backfilled with argon at room temperature. Between 0.3 mL and 0.5 mL of each solution was removed for analysis by $^{31}P\{^1H\}$ NMR spectroscopy, which showed that each mixture contained approximately 50% [Rh(DPEphos)$(H)_2(NMeH_2)_2$][BAr^F_4] (**5**) and 50% [Rh(DPEphos)$(NMeH_2)_2$][BAr^F_4] (**6**). A further 0.5 mL of each reaction mixture (containing approximately 2.2 µmol, 4.5 µmol and 11.2 µmol for 0.2 mol%, 0.4 mol% and 1.0 mol% **5**/**6** respectively) was removed via syringe and used as catalysts for $H_3B{\cdot}NMeH_2$ dehydropolymerization under hydrogen evolution measurements conditions as per the general procedure (vide supra).

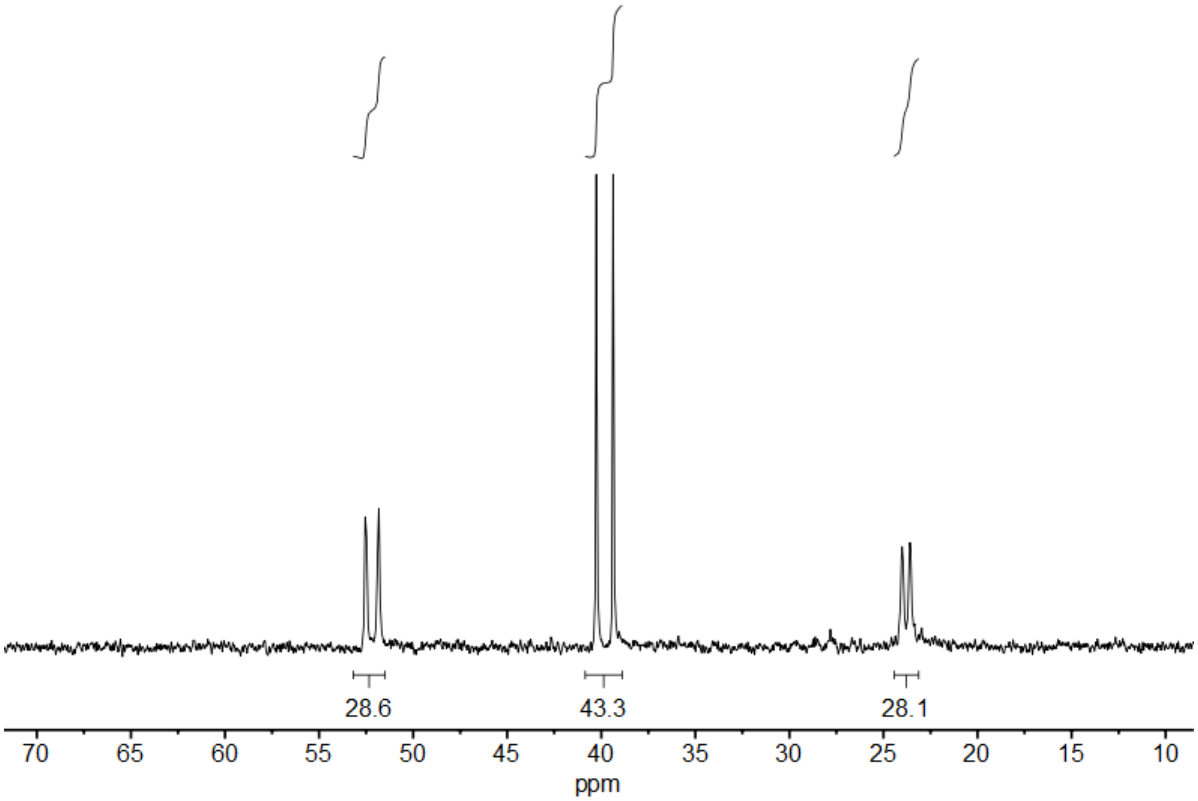

Figure S17. Representative $^{31}P\{^{1}H\}$ NMR spectrum of an in situ formed mixture of complexes **5/6** used as a catalyst in $H_3B{\cdot}NMeH_2$ dehydropolymerization.

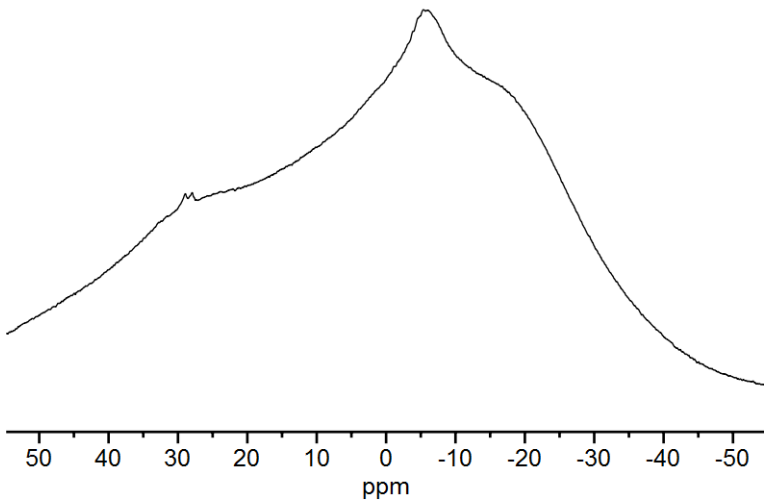

Figure S18. Representative ^{11}B NMR spectrum (1,2–$F_2C_6H_4$ solvent, 298 K) of the dehydropolymerization reaction mixture using **2a** under open conditions. 0.2 mol% **2a**, [**2a**] = 4.45×10^{-4} M, [$H_3B{\cdot}NMeH_2$] = 0.223 M, 1,2–$F_2C_6H_4$ solvent, open conditions. The broad baseline signal observed in the ^{11}B NMR spectrum at δ ~20.0 is due to background from the tube and probe (borosilicate glass).

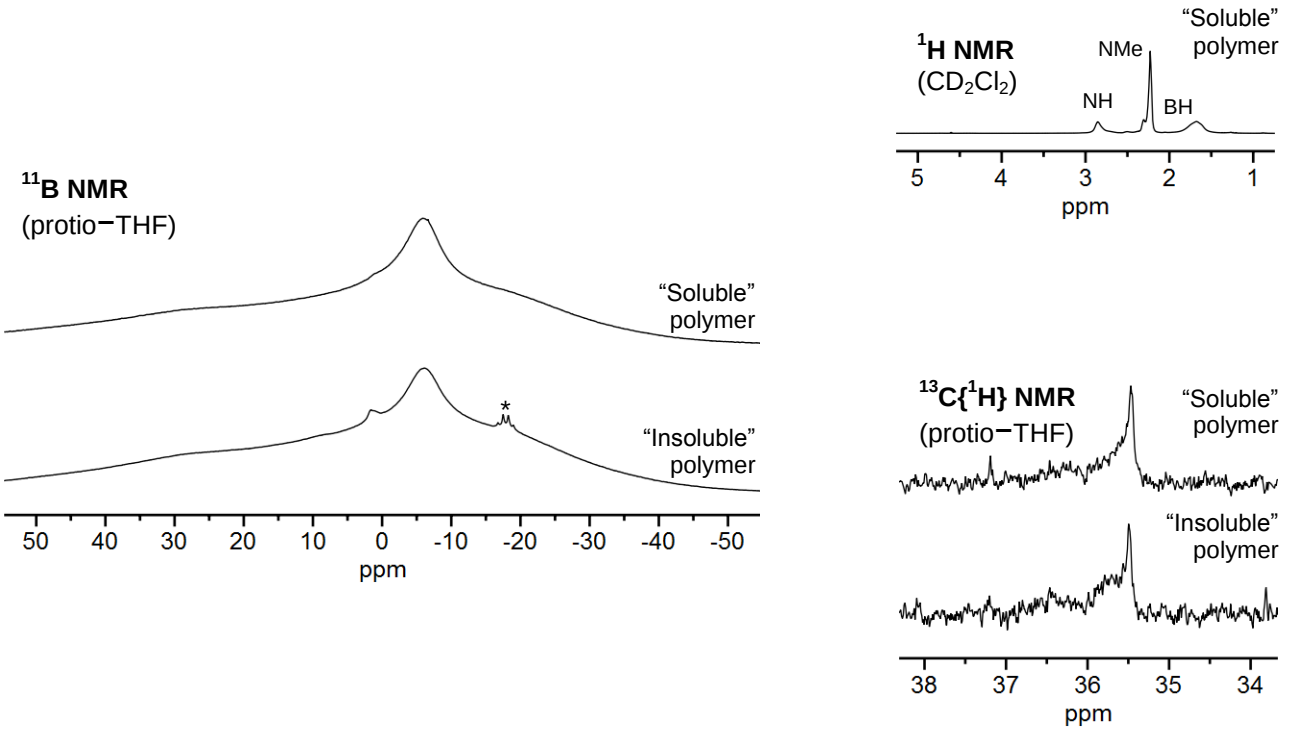

Figure S19. NMR spectra (protio−THF solvent unless otherwise stated, 298 K) for isolated $(H_2BNMeH)_n$ produced by **2a**. "Soluble" polymer is $(H_2BNMeH)_n$ that is soluble in 1,2–$F_2C_6H_4$, CD_2Cl_2 and THF solvents. "Insoluble" polymer is $(H_2BNMeH)_n$ that is insoluble in 1,2–$F_2C_6H_4$ and CD_2Cl_2 solvents, but is soluble in THF solvent. Direct comparison between "soluble" and "insoluble" polymer by NMR spectroscopy can be carried out in THF solvent, and indicates that "insoluble" polymer may demonstrate greater cross linking/chain branching than "soluble" polymer due to greater intensity peaks at δ ~1.0 in the ^{11}B NMR spectrum and at δ ~35.7 in the $^{13}C\{^{1}H\}$ NMR spectrum. These may signal tertiary or quaternary main chain centers.[3] The broad baseline signals observed in the ^{11}B NMR spectra at δ ~20.0 are due to background from the tube and probe (borosilicate glass). * = entrained $H_3B{\cdot}NMeH_2$ or polymeryl–BH_3 end group. Note that all reported GPC data are for unseparated "soluble" and "insoluble" polymer mixtures in order to directly compare all samples produced under different conditions – note that THF solvent is used for GPC analysis.

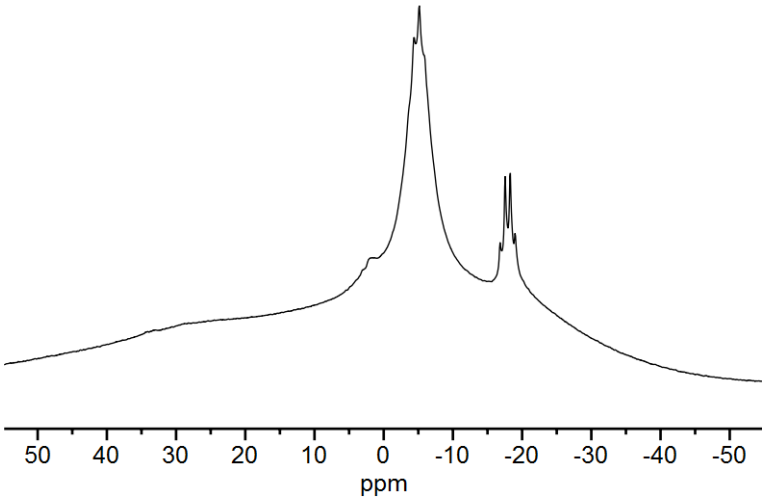

Figure S20. ^{11}B NMR spectrum (protio–THF solvent, 298 K) for isolated $(H_2BNMeH)_n$ produced by **2a** under closed conditions. 0.4 mol% **2a**, [**2a**] = 8.92×10^{-4} M, $[H_3B{\cdot}NMeH_2]$ = 0.223 M, 1,2–$F_2C_6H_4$ solvent, closed conditions. The broad baseline signal observed in the ^{11}B NMR spectrum at δ ~20.0 is due to background from the tube and probe (borosilicate glass). GPC analysis of $(H_2BNMeH)_n$: M_n = 5,700 g/mol, Đ = 2.0.

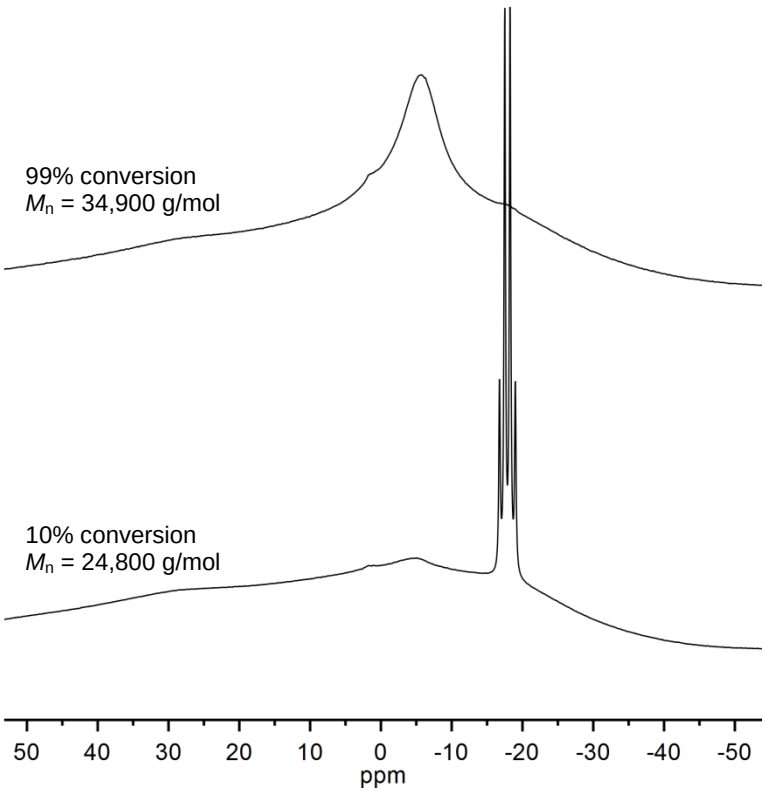

Figure S21. Stacked ^{11}B NMR spectra (protio−THF solvent, 298 K) of isolated $(H_2BNMeH)_n$ samples from the dehydropolymerization of $H_3B{\cdot}NMeH_2$ under molecular

weight vs conversion conditions. 0.2 mol% **2a**, [**2a**] = 4.45×10^{-4} M, [$H_3B{\cdot}NMeH_2$] = 0.223 M, 1,2–$F_2C_6H_4$ solvent, open conditions, at 99% $H_3B{\cdot}NMeH_2$ conversion (top) and 10% $H_3B{\cdot}NMeH_2$ conversion (bottom). The broad baseline signals observed at δ ~20.0 are due to background from the tube and probe (borosilicate glass). The signal at δ −18.0 is due to unreacted $H_3B{\cdot}NMeH_2$. The ^{11}B NMR spectra were back−linear corrected and the signals pertaining to $H_3B{\cdot}NMeH_2$ (δ −18.0) and $(H_2BNMeH)_n$ (δ −6.0) were integrated with respect to one another to determine the % conversion.

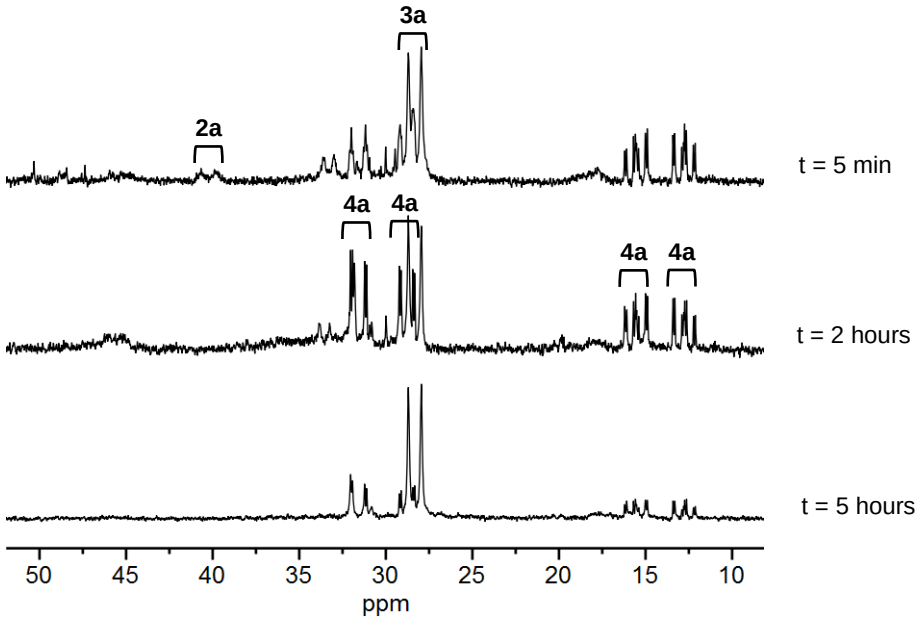

Figure S22. Stacked $^{31}P\{^1H\}$ NMR spectra (1,2–$F_2C_6H_4$ solvent, 298 K) of the reaction of $H_3B{\cdot}NMeH_2$ with 10 mol% **2a** in 1,2–$F_2C_6H_4$ solvent over time. The doublet at δ 28.3 shows the phosphorus environment of **3a**. The multiplets at δ 31.7, δ 28.9, δ 15.7 and δ 12.8 are the phosphorus environments of **4a**.

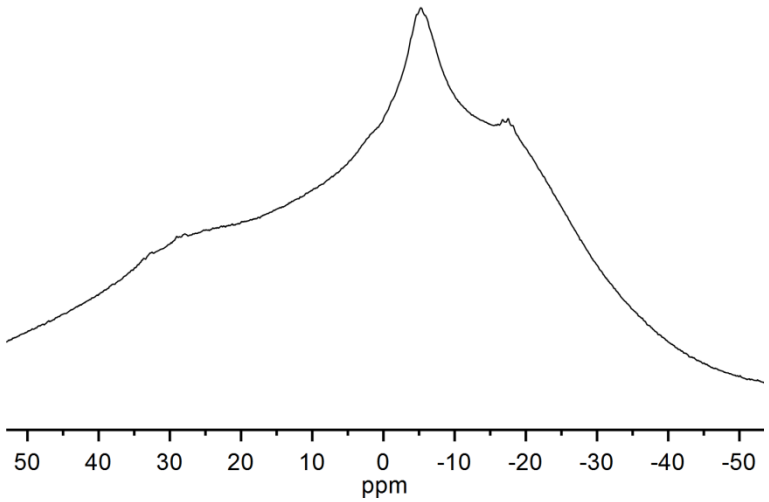

Figure S23. Representative ^{11}B NMR spectrum (1,2–$F_2C_6H_4$, 298 K) of the dehydropolymerization reaction mixture using **2a** under hydrogen evolution measurement conditions. 0.2 mol% **2a**, [**2a**] = 4.45 × 10^{-4} M, [$H_3B{\cdot}NMeH_2$] = 0.223 M, 1,2–$F_2C_6H_4$ solvent, hydrogen evolution measurement conditions. The broad baseline signal observed in the ^{11}B NMR spectrum at δ ~20.0 is due to background from the tube and probe (borosilicate glass).

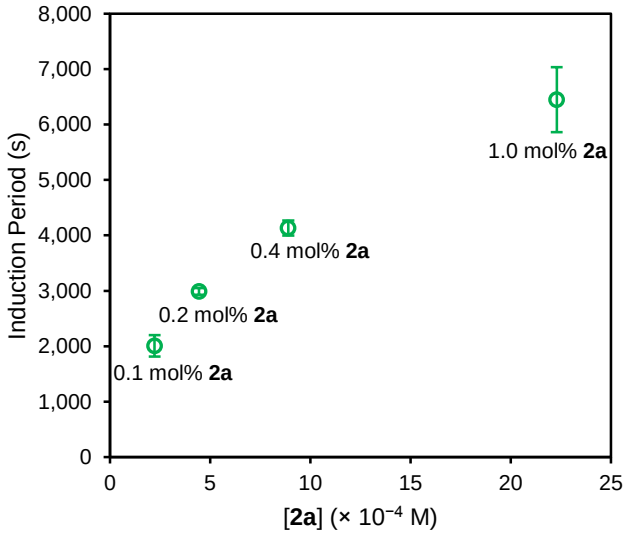

Figure S24. Induction period prior to the onset on hydrogen evolution vs [**2a**] plot for the dehydropolymerization of $H_3B{\cdot}NMeH_2$ using **2a** (as measured by hydrogen evolution). [$H_3B{\cdot}NMeH_2$] = 0.223 M, 1,2–$F_2C_6H_4$ solvent, hydrogen evolution measurement conditions.

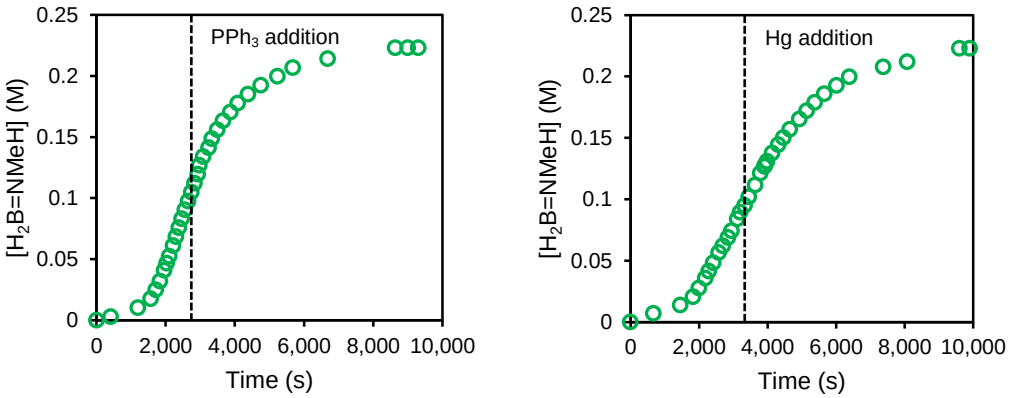

Figure S25. Temporal data plots for $H_2B{=}NMeH$ formation (as measured by hydrogen evolution). 0.4 mol% **2a**, [**2a**] = 8.92×10^{-4} M, [$H_3B{\cdot}NMeH_2$] = 0.223 M, 1,2–$F_2C_6H_4$ solvent, hydrogen evolution measurement conditions. Left: Effect of 0.2 equivs. of PPh_3 added at 2,800 s. Right: Effect of 1,500 equivs. of Hg added at 3,600 s.

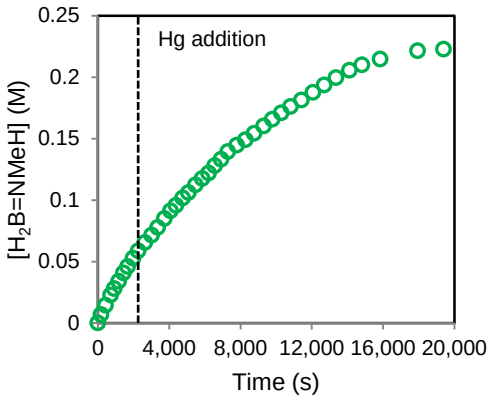

Figure S26. Temporal data plots for $H_2B{=}NMeH$ formation (as measured by hydrogen evolution). 0.2 mol% **6**, [**6**] = 4.45×10^{-4} M, [$H_3B{\cdot}NMeH_2$] = 0.223 M, 1,2–$F_2C_6H_4$ solvent, hydrogen evolution measurement conditions. Effect of 1,500 equivs. of Hg added at 2,600 s.

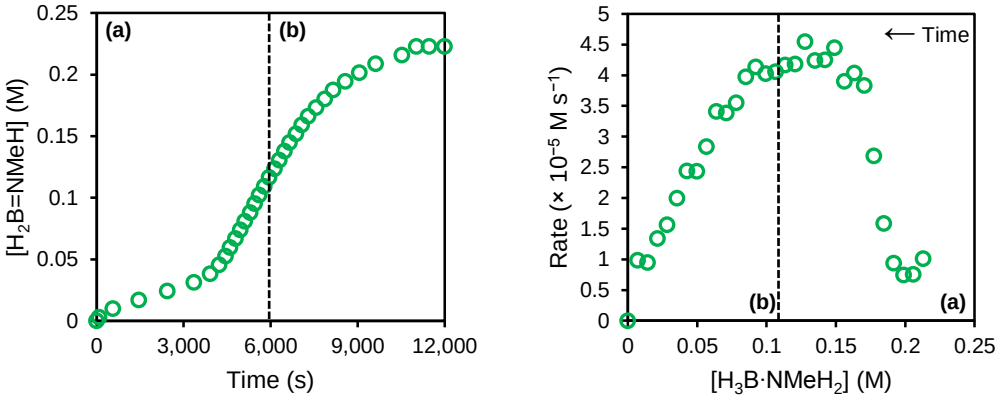

Figure S27. Left: Temporal data plot for $H_2B{=}NMeH$ formation (as measured by hydrogen evolution). 0.4 mol% **2a**, [**2a**] = 8.92 × 10^{-4} M, $[H_3B{\cdot}NMeH_2]$ = 0.223 M, 1,2–$F_2C_6H_4$ solvent, hydrogen evolution measurement conditions. Right: Rate vs $[H_3B{\cdot}NMeH_2]$ over time. 0.4 mol% **2a**, [**2a**] = 8.92 × 10^{-4} M, $[H_3B{\cdot}NMeH_2]$ = 0.223 M, 1,2–$F_2C_6H_4$ solvent, hydrogen evolution measurement conditions. **(a)** Acceleration phase. **(b)** Deceleration phase.

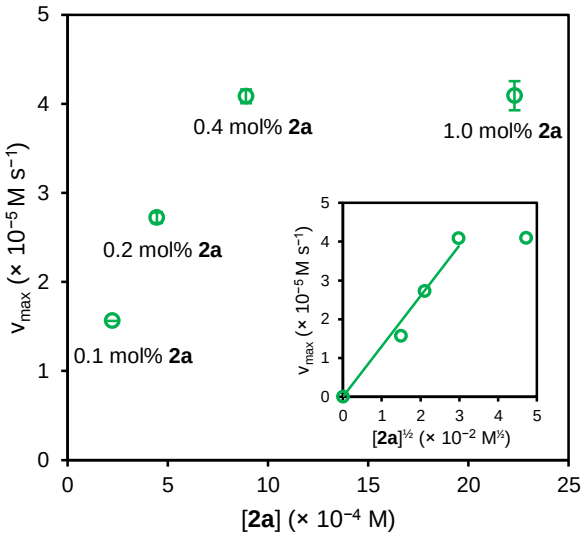

Figure S28. v_{max} (maximum rate) vs [**2a**] plot for the dehydropolymerization of $H_3B{\cdot}NMeH_2$ using **2a** (as measured by hydrogen evolution). $[H_3B{\cdot}NMeH_2]$ = 0.223 M, 1,2–$F_2C_6H_4$ solvent, hydrogen evolution measurement conditions. Inset: v_{max} (maximum rate) vs $[\mathbf{2a}]^{1/2}$ plot for the dehydropolymerization of $H_3B{\cdot}NMeH_2$ using **2a**. $[H_3B{\cdot}NMeH_2]$ = 0.223 M, 1,2–$F_2C_6H_4$ solvent, hydrogen evolution measurement conditions. A line of best fit is shown for a hypothetical half order dependence on [**2a**] between 2.23 × 10^{-4} M and 8.92 × 10^{-4} M **2a** (0.1 mol% and 0.4 mol% **2a**) (R^2 = 0.979).

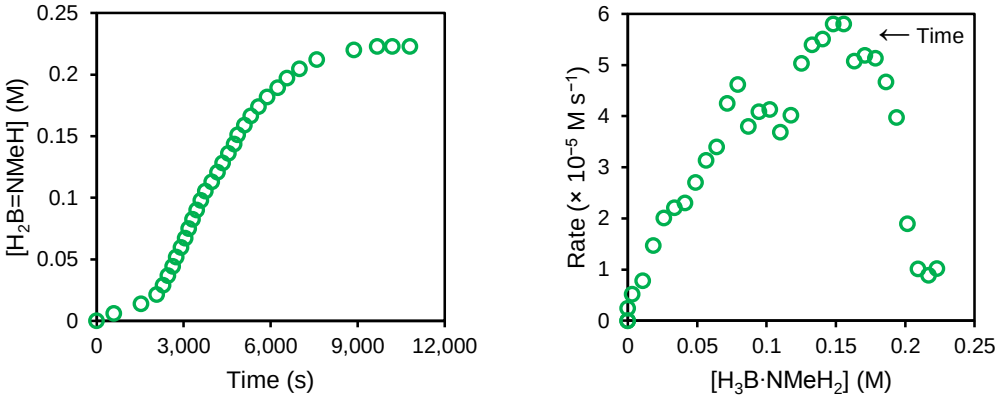

Figure S29. Left: Temporal data plot for $H_2B{=}NMeH$ formation (as measured by hydrogen evolution). 0.2 mol% in situ formed **3a** (0.4 mol% with respect to Rh_{TOTAL}), [**3a**] = 4.45×10^{-4} M ($[Rh]_{TOTAL} = 8.92 \times 10^{-4}$ M), $[H_3B{\cdot}NMeH_2]$ = 0.223 M, 1,2–$F_2C_6H_4$ solvent, hydrogen evolution measurement conditions. Right: Rate vs $[H_3B{\cdot}NMeH_2]$ over time. 0.2 mol% in situ formed **3a** (0.4 mol% with respect to Rh_{TOTAL}), [**3a**] = 4.45×10^{-4} M ($[Rh]_{TOTAL} = 8.92 \times 10^{-4}$ M), $[H_3B{\cdot}NMeH_2]$ = 0.223 M, 1,2–$F_2C_6H_4$ solvent, hydrogen evolution measurement conditions.

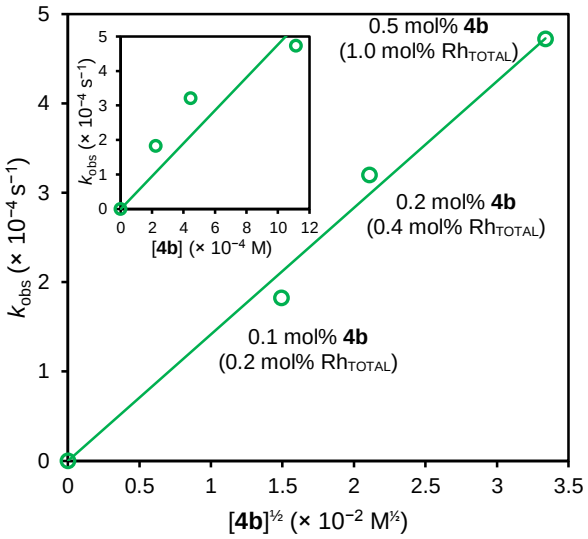

Figure S30. First order k_{obs} vs $[\mathbf{4b}]^{½}$ plot for the dehydropolymerization of $H_3B{\cdot}NMeH_2$ using **4b** (as measured by hydrogen evolution). $[H_3B{\cdot}NMeH_2]$ = 0.223 M, 1,2–$F_2C_6H_4$ solvent, hydrogen evolution measurement conditions. A line of best fit is shown for the proposed half order dependence on [**4b**] (R^2 = 0.989). Inset: First order k_{obs} vs [**4b**] plot for the dehydropolymerization of $H_3B{\cdot}NMeH_2$ using **4b**. $[H_3B{\cdot}NMeH_2]$ = 0.223 M, 1,2–$F_2C_6H_4$ solvent, hydrogen evolution measurement conditions. A line of best fit is shown for a hypothetical first order dependence on [**4b**] (R^2 = 0.827).

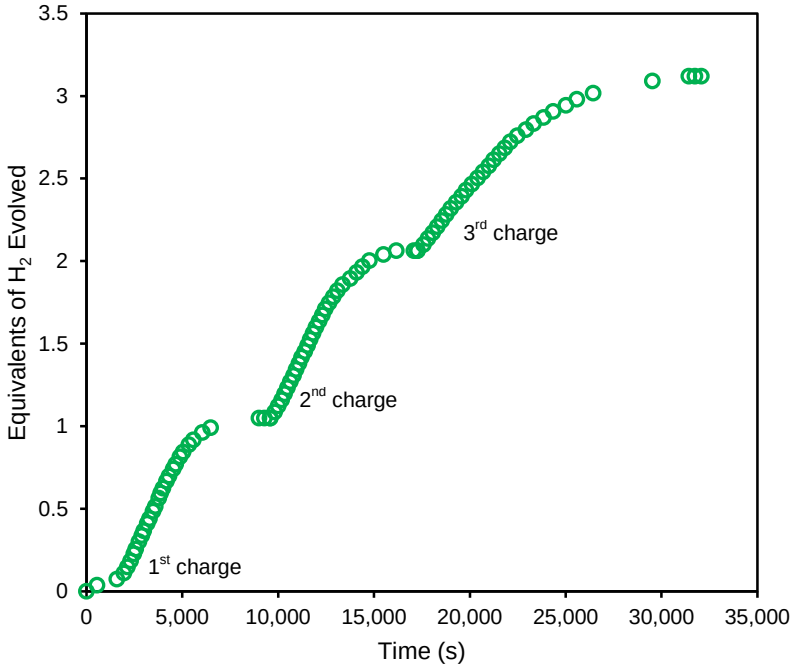

Figure S31. Temporal data plots for the equivalents of H_2 formed over 3 successive catalytic runs (as measured by hydrogen evolution). 0.4 mol% **2a**, [**2a**] = 8.92×10^{-4} M, [$H_3B{\cdot}NMeH_2$] = 0.223 M × 3, 1,2–$F_2C_6H_4$ solvent, hydrogen evolution measurement conditions. GPC analysis of $(H_2BNMeH)_n$ at the end of the 3rd charge: M_n = 9,500 g/mol, Đ = 1.8.

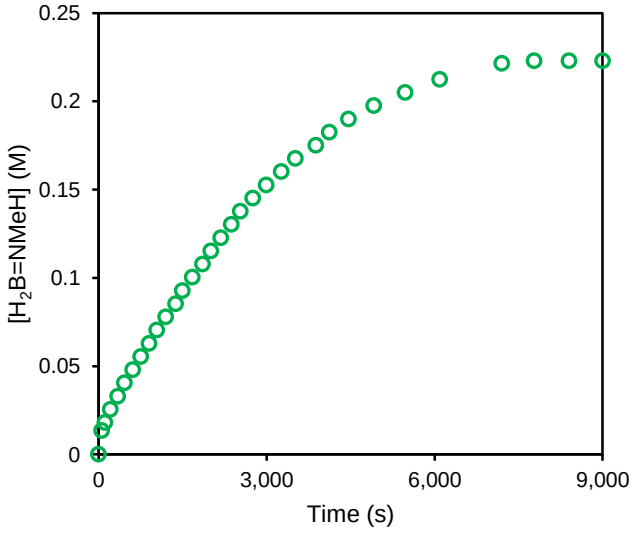

Figure S32. Temporal data plot for H_2B=NMeH formation (as measured by hydrogen evolution). 0.4 mol% **2a**, [**2a**] = 8.92×10^{-4} M, [$H_3B{\cdot}NMeH_2$] = 0.223 M, 1,2–$F_2C_6H_4$ solvent, 0.05 mL (50 µL) of a THF solution containing ~2 equivs. $NMeH_2$ with respect to **2a** was added into the reaction vessel after 5 seconds, hydrogen evolution measurement conditions.

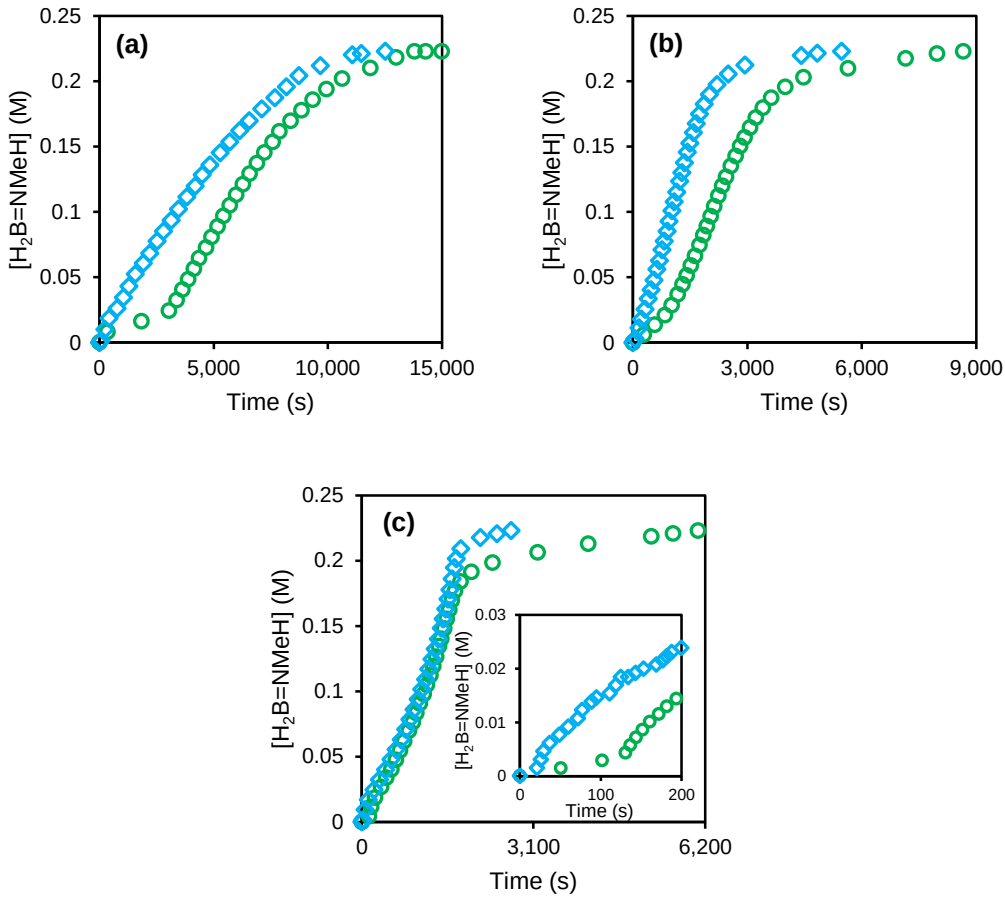

Figure S33. Temporal data plots for $H_2B{=}NMeH$ formation (as measured by hydrogen evolution). 0.2 mol% catalyst, [catalyst] = 4.45×10^{-4} M, [$H_3B{\cdot}NMeH_2$] = 0.223 M, 1,2–$F_2C_6H_4$ solvent, with and without 0.05 mL (50 μL) of a THF solution containing ~2 equivs. $NMeH_2$ with respect to catalyst added into the reaction vessel after 5 seconds, hydrogen evolution measurement conditions. **(a)** Catalyst = [Rh(DPEphos)(η^2–$H_2B(NMe_3)(CH_2)_2{}^tBu$)][$BAr^F{}_4$] (**2a**). **(b)** Catalyst = [Rh(Xantphos–Ph)(η^2–$H_2B(NMe_3)(CH_2)_2{}^tBu$)][$BAr^F{}_4$] (**A**). **(c)** Catalyst = [$Rh(Ph_2P(CH_2)_3PPh_2)(C_6H_5F)$][$BAr^F{}_4$]. Inset: Expansion of the region between 0 and 200 s, showing the induction period of ca. 100 s prior to the onset of hydrogen evolution without $NMeH_2$, and lack of induction period with ~2 equivs. $NMeH_2$ added. ○ = No added $NMeH_2$; ◇ = doped with ~2 equivs. $NMeH_2$.

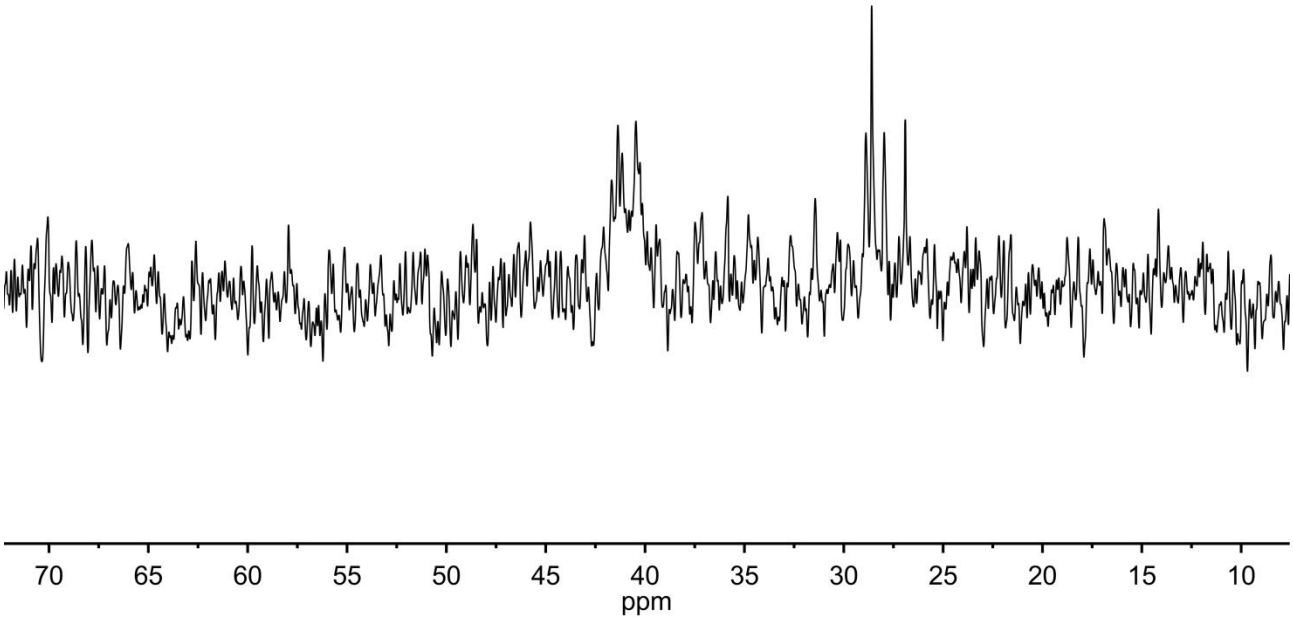

Figure S34. $^{31}P\{^{1}H\}$ NMR spectrum (1,2–$F_2C_6H_4$ solvent, 298 K) of the reaction mixture upon completion of productive catalysis using 0.5 mol% $[Rh_2(DPEphos)_2(\sigma,\mu–(H_2B)_2NHMe)][Al(OC(CF_3)_3)_4]$ (**4b**).

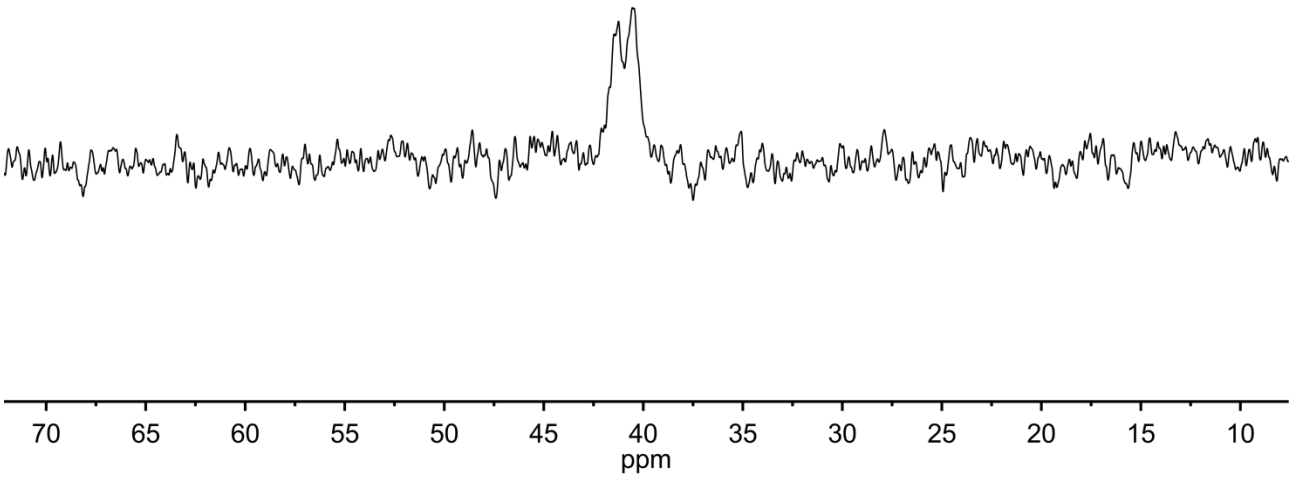

Figure S35. $^{31}P\{^{1}H\}$ NMR spectrum (1,2–$F_2C_6H_4$ solvent, 298 K) of the reaction mixture during productive catalysis using 1 mol% $[Rh(DPEphos)(NMeH_2)_2][BAr^F{}_4]$ (**6**).

Computational Details

The geometry optimization of **4b** was run with Gaussian 03 Revision D.01[17] and performed using the BP86[18–19] functional. Rh and P centres were described with Stuttgart RECPs and associated basis sets,[20] with added d–orbital polarization on P (ζ = 0.387)[21] and 6–31G** basis sets for C, H, O, B and N.[22–23] Stationary points were fully characterized via analytical frequency calculations as minima with all positive eigenvalues. Atoms in Molecules[24] analyses were performed with the AIMALL program[25] using the same functional and basis sets described above.

Geometry Optimization of 4b

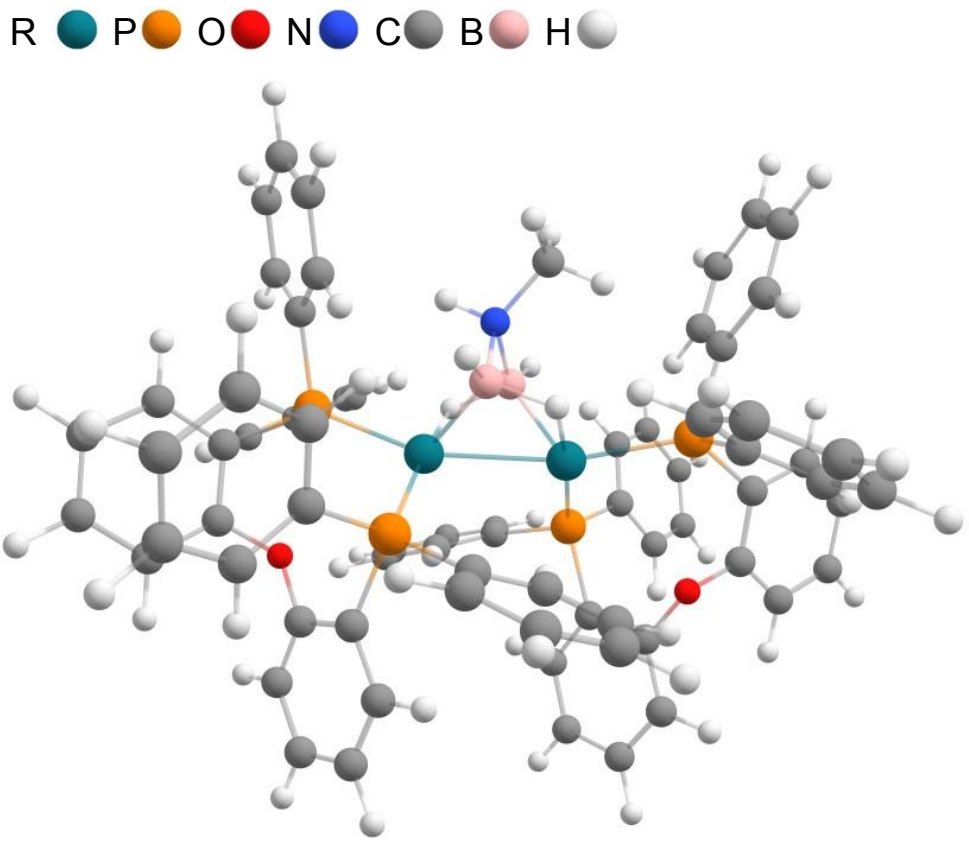

Figure S36. Geometry optimized structure of the cationic portion of **4b**.

Table S1. Comparison of key distances between the experimental (Fig. 2a) and computed (Fig. S18) structures of the cationic portion of **4b**.

Bond	Computed Distance (Å)	Crystal Structure (Å)
Rh1–Rh2	2.70	2.6421(4)
Rh1–B1	2.37	2.326(5)
Rh1–B2	2.11	2.096(5)
Rh2–B1	2.11	2.107(5)
Rh2–B2	2.34	2.328(5)
Rh1–C38	2.99	2.998(4)
B1–N1	1.59	1.59(1)
B2–N1	1.57	1.56(1)

Quantum Theory of Atoms in Molecules (QTAIM) Analysis of **4b**

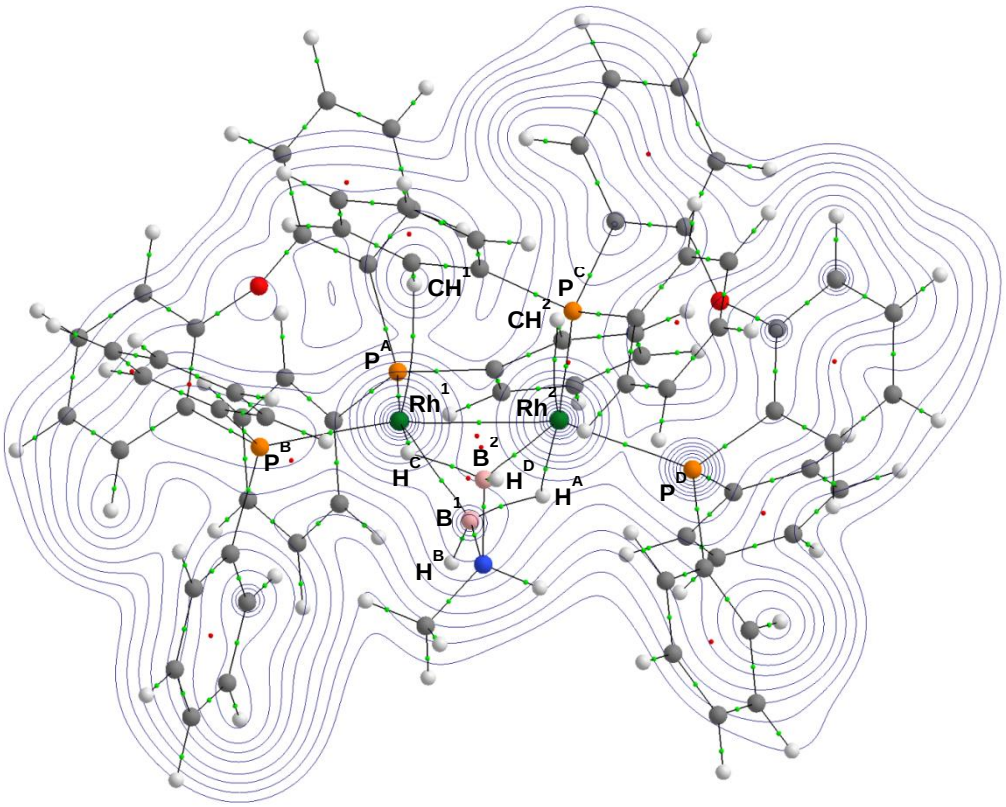

Figure S37. Molecular graph of the cationic portion of **4b** with 2D contour plot of the electron density present with projected stationary points and bond paths. Bond critical points (BCPs) are shown in green and ring critical points in red.

Table S2. Calculated QTAIM parameters (a.u.) for selected BCPs in **4b**. ρ(r) = electron density, $\nabla^2\rho(r)$ = Laplacian of the electron density, ε = bond ellipticity, H(r)= total energy density.

BCP	ρ(r)	$\nabla^2\rho(r)$	ε	H(r)	BCP	ρ(r)	$\nabla^2\rho(r)$	ε	H(r)
Rh^1–Rh^2	0.05	0.08	0.32	−0.02	Rh^2–B^2	0.10	−0.06	0.10	−0.05
Rh^1–H^CB^2	0.10	0.25	0.39	−0.04	B^1–H^B	0.17	−0.25	0.03	−0.18
Rh^2–H^AB^1	0.09	0.25	0.39	−0.03	B^2–H^D	0.17	−0.24	0.03	−0.18
B^2–H^C	0.12	−0.13	0.40	−0.10	Rh^1–HC	0.02	0.06	0.28	0.00
B^1–H^A	0.12	−0.12	0.32	−0.11	Rh^2–HC	0.02	0.07	0.37	0.00
Rh^1–B^1	0.10	−0.06	0.10	−0.05					

XYZ Coordinates of ***4b***

SCF Energy = −3322.72757080
Enthalpy 0 K = −3321.589126
Enthalpy 298 K = −3321.509993
Free Energy 298 K = −3321.707704
Lowest Frequencies = 11.230, 17.760 cm^{-1}

C	3.444857000	0.351569000	3.563810000
C	3.829667000	−0.826665000	2.884262000
C	4.440204000	−1.866978000	3.618225000
C	4.654313000	−1.730571000	5.000284000
C	4.268563000	−0.556445000	5.666920000
C	3.667332000	0.487544000	4.944314000
P	3.511198000	−0.943889000	1.040425000
Rh	1.333465000	−0.189685000	0.378031000
Rh	−1.349177000	0.135695000	0.448915000
P	−3.597755000	0.723258000	1.087748000
C	−5.049834000	0.125338000	0.080299000
C	−4.942276000	0.164372000	−1.325946000
C	−5.981476000	−0.275836000	−2.158819000
C	−7.162191000	−0.762764000	−1.577885000
C	−7.300248000	−0.803332000	−0.181544000
C	−6.251038000	−0.359238000	0.638349000
O	−3.767122000	0.726447000	−1.833361000
C	−3.195178000	0.153944000	−2.974118000
C	−2.273360000	−0.909070000	−2.829594000
C	−1.689011000	−1.422113000	−4.008901000
C	−1.996568000	−0.885371000	−5.269733000
C	−2.890038000	0.190401000	−5.379888000
C	−3.491809000	0.714271000	−4.225403000
P	−1.804067000	−1.552170000	−1.119757000
C	−0.394470000	−2.698806000	−1.572238000
C	−0.569829000	−4.090842000	−1.714684000
C	0.500675000	−4.904268000	−2.124700000
C	1.754582000	−4.339011000	−2.400594000
C	1.939746000	−2.954129000	−2.260809000
C	0.873339000	−2.139570000	−1.846788000
C	5.045311000	−0.169426000	0.324923000
C	5.065990000	0.079949000	−1.064388000
C	6.167976000	0.680129000	−1.689528000
C	7.278864000	1.040209000	−0.911046000
C	7.286054000	0.799259000	0.472196000
C	6.175444000	0.196372000	1.083518000
O	3.952442000	−0.373814000	−1.774857000
C	3.450149000	0.384818000	−2.836708000
C	2.470385000	1.374546000	−2.583989000
C	1.930972000	2.051430000	−3.699634000
C	2.343473000	1.747856000	−5.007612000
C	3.303667000	0.750091000	−5.230711000
C	3.857414000	0.062233000	−4.139711000
P	1.898815000	1.736410000	−0.824314000
C	3.250382000	2.881906000	−0.209425000

C	3.233628000	3.283948000	1.143024000
C	4.160257000	4.222970000	1.621356000
C	5.118138000	4.773748000	0.754428000
C	5.137092000	4.385613000	−0.594008000
C	4.206939000	3.449534000	−1.076192000
C	0.533186000	2.977471000	−1.141645000
C	0.759053000	4.369686000	−1.109747000
C	−0.282660000	5.265122000	−1.406775000
C	−1.557135000	4.782646000	−1.741249000
C	−1.791528000	3.398389000	−1.774815000
C	−0.753312000	2.502138000	−1.474985000
C	3.823678000	−2.768738000	0.741589000
C	2.848912000	−3.705438000	1.149887000
C	3.074895000	−5.081582000	1.000597000
C	4.270270000	−5.543045000	0.423757000
C	5.239711000	−4.619141000	0.004037000
C	5.022886000	−3.240036000	0.167921000
B	−0.321502000	−1.157807000	1.769104000
N	0.153630000	−0.214037000	2.952654000
B	0.343256000	0.927354000	1.869191000
C	−0.732660000	0.008938000	4.127902000
C	−3.147553000	−2.805360000	−0.762321000
C	−3.116582000	−3.469832000	0.483513000
C	−4.038157000	−4.489354000	0.769492000
C	−5.007132000	−4.851948000	−0.181091000
C	−5.040712000	−4.198156000	−1.422309000
C	−4.111188000	−3.186140000	−1.716945000
C	−3.908473000	2.574834000	1.118368000
C	−2.915601000	3.440882000	1.625406000
C	−3.153076000	4.820789000	1.724459000
C	−4.379337000	5.358859000	1.301483000
C	−5.369012000	4.507316000	0.785404000
C	−5.139672000	3.124099000	0.699855000
C	−4.118338000	0.224201000	2.814634000
C	−4.506923000	1.162453000	3.793692000
C	−4.854494000	0.734580000	5.087293000
C	−4.831360000	−0.630149000	5.413229000
C	−4.457008000	−1.571583000	4.438380000
C	−4.094995000	−1.148087000	3.151205000
H	−2.350559000	−3.202806000	1.219518000
H	1.175283000	2.826443000	−3.542191000
H	−1.543938000	−4.546755000	−1.517472000
H	2.588946000	−4.974290000	−2.715958000
H	−3.995424000	−5.004171000	1.735996000
H	1.089615000	−0.483651000	3.298808000
H	1.905060000	−3.361385000	1.586782000
H	−0.978044000	−2.250206000	−3.939551000
H	1.906731000	2.292350000	−5.851296000
H	4.598774000	−0.730701000	−4.282598000
H	2.916157000	−2.502424000	−2.456074000
H	8.144763000	1.505976000	−1.393760000
H	0.345687000	−5.983581000	−2.233011000

H	−4.136470000	−2.700226000	−2.696949000
H	4.751076000	−2.785795000	3.111787000
H	1.009904000	−1.045538000	−1.778847000
H	−5.866426000	−0.234297000	−3.246181000
H	−2.784829000	3.008127000	−2.014289000
H	2.470549000	2.880447000	1.815114000
H	6.154542000	0.860055000	−2.768899000
H	5.799297000	−2.532991000	−0.140875000
H	−6.362233000	−0.392875000	1.726404000
H	4.445167000	−6.617919000	0.304008000
H	3.622208000	0.502131000	−6.248727000
H	−0.932163000	1.414003000	−1.516520000
H	1.748662000	4.762018000	−0.859001000
H	−2.369405000	5.481732000	−1.967370000
H	8.155560000	1.077450000	1.076445000
H	4.129535000	4.528056000	2.673371000
H	−8.224117000	−1.176605000	0.272059000
H	−7.978687000	−1.103146000	−2.223867000
H	−5.728307000	−5.645534000	0.042791000
H	2.310365000	−5.793893000	1.329592000
H	−0.090738000	6.343535000	−1.377235000
H	−4.189621000	1.556270000	−4.277540000
H	5.128165000	−2.547501000	5.555700000
H	−3.802925000	−1.885440000	2.396548000
H	6.182023000	0.009993000	2.162213000
H	−1.946887000	3.040240000	1.940871000
H	6.177173000	−4.968600000	−0.443006000
H	−5.929155000	2.471738000	0.313814000
H	2.981345000	1.168372000	3.001153000
H	−4.542092000	2.228687000	3.550620000
H	−3.122368000	0.622758000	−6.358882000
H	−1.527547000	−1.307571000	−6.164595000
H	−5.788147000	−4.479265000	−2.172336000
H	4.437418000	−0.454432000	6.744408000
H	−4.562686000	6.436587000	1.373588000
H	−4.444403000	−2.639984000	4.681792000
H	−2.371400000	5.475936000	2.124297000
H	−5.152558000	1.475053000	5.837896000
H	3.370275000	1.410958000	5.454232000
H	−6.330175000	4.916351000	0.454374000
H	−5.107609000	−0.960674000	6.420461000
H	−0.851294000	−0.931376000	4.691707000
H	−1.720221000	0.339634000	3.778758000
H	−0.296296000	0.784180000	4.779990000
H	0.791823000	1.978582000	2.291752000
H	−0.842249000	−2.204151000	2.110172000
H	−0.888825000	1.382446000	1.528223000
H	0.794420000	−1.628808000	1.171740000
H	4.224598000	3.171176000	−2.134249000
H	5.875356000	4.815035000	−1.280269000
H	5.842130000	5.506615000	1.126948000

Crystallography

Single crystal X–ray diffraction data for **4b** was collected as follows: a typical crystal was mounted on a MiTeGen Micromounts using perfluoropolyether oil and cooled rapidly to 150(1) K in a stream of nitrogen gas using an Oxford Cryosystems Cryostream unit.[26] Data were collected with an Agilent SuperNova diffractometer (Cu K_α radiation, λ = 1.54180 Å). Raw frame data were reduced using CrysAlisPro.[27] The structures were solved using SHELXT[28] and refined using full–matrix least squares refinement on all F^2 data using the SHELXL[29] (version 2014/7) using the interface OLEX2.[30] Hydrides were located in the difference map and refined isotropically. All other hydrogen atoms were placed in calculated positions (riding model). All $OC(CF_3)_3$ moieties and the N(H)Me unit exhibited disorder. This was treated by employing a split site model, restraints to bond lengths and displacement ellipsoids were applied. Highly disordered lattice solvent molecules could not be satisfactorily modeled. The solvent masking algorithm in OLEX2 was applied, structure factors for 176 electrons in 740 Å^3 per unit cell were introduced. On the basis of the electron count the void is suspected of containing three 1,2–difluorobenzene molecules, however this has not been included in the atom list or molecular formula. Thus all calculated quantities that derive from the molecular formula are known to be incorrect.

Table S3. Crystallographic data for complex **4b**.

Complex	**4b**
Chemical formula	$C_{89}H_{64}Al_1B_2F_{36}N_1O_6P_4Rh_2$
Formula weight (g/mol)	2305.71
Temperature (K)	150(1)
Crystal system	Triclinic
Space group	*P*−1
a (Å)	14.5138(2)
b (Å)	18.5644(3)
c (Å)	21.4620(3)
α (deg)	104.385(1)
β (deg)	102.683(1)
γ (deg)	107.545(1)
V (Å^3)	5062.15(13)
Z	2
ρ (calcd) (g cm^{-3})	1.513
μ (mm^{-1})	4.361
Reflections collected	59615
Unique reflections	20909
Restraints/parameters	2901/1761
R_{int}	0.0477
R_1 [$I > 2\sigma(I)$]	0.0579
wR_2 [$I > 2\sigma(I)$]	0.1729
GoF	1.030
Residual electron density (e Å^{-3})	1.76, −0.94
CCDC no.	1877231

References

(1) Pangborn, A. B.; Giardello, M. A.; Grubbs, R. H.; Rosen, R. K.; Timmers, F. J., Safe and Convenient Procedure for Solvent Purification. *Organometallics* **1996**, *15*, 1518–1520.

(2) Buschmann, W. E.; Miller, J. S., Synthesis of $[M^{II}(NCMe)_6]^{2+}$ (M = V, Cr, Mn, Fe, Co, Ni) Salts of Tetra[3,5–bis(trifluoromethyl)phenyl]borate. *Inorg. Synth.* **2002**, *33*, 83–91.

(3) Adams, G. M.; Colebatch, A. L.; Skornia, J. T.; McKay, A. I.; Johnson, H. C.; Lloyd–Jones, G. C.; Macgregor, S. A.; Beattie, N. A.; Weller, A. S., Dehydropolymerization of $H_3B{\cdot}NMeH_2$ To Form Polyaminoboranes Using [Rh(Xantphos–alkyl)] Catalysts. *J. Am. Chem. Soc.* **2018**, *140*, 1481–1495.

(4) Colebatch, A. L.; Hawkey Gilder, B. W.; Whittell, G. R.; Oldroyd, N. L.; Manners, I.; Weller, A. S., A General, Rhodium-Catalyzed, Synthesis of Deuterated Boranes and *N*-Methyl Polyaminoboranes. *Chem. Eur. J.* **2018**, *24*, 5450–5455.

(5) Moxham, G. L.; Randell–Sly, H. E.; Brayshaw, S. K.; Woodward, R. L.; Weller, A. S.; Willis, M. C., A Second–Generation Catalyst for Intermolecular Hydroacylation of Alkenes and Alkynes Using β–S–Substituted Aldehydes: The Role of a Hemilabile P–O–P Ligand. *Angew. Chem. Int. Ed.* **2006**, *45*, 7618–7622.

(6) Hooper, J. F; Chaplin, A. B., González−Rodríguez, C.; Thompson, A. L.; Weller, A. S.; Willis, M. C., Aryl Methyl Sulfides as Substrates for Rhodium–Catalyzed Alkyne Carbothiolation: Arene Functionalization with Activating Group Recycling. *J. Am. Chem. Soc.* **2012**, *134*, 2906–2909.

(7) Esteruelas, M. A.; Oliván, M.; Vélez A., Xantphos−Type Complexes of Group 9: Rhodium versus Iridium. *Inorg. Chem.* **2013**, *52*, 5339–5349.

(8) Johnson, H. C.; McMullin, C. L.; Pike, S. D.; Macgregor, S. A.; Weller A. S., Dehydrogenative Boron Homocoupling of an Amine–Borane. *Angew. Chem. Int. Ed.* **2013**, *52*, 9776–9780.

(9) Dallanegra, R.; Robertson, A. P. M.; Chaplin, A. B.; Manners, I.; Weller, A. S., Tuning the $[L_2Rh{\cdots}H_3B{\cdot}NR_3]^+$ interaction using phosphine bite angle. Demonstration by the catalytic formation of polyaminoboranes. *Chem. Commun.* **2011**, *47*, 3763–3765.

(10) Colebatch, A. L.; McKay, A. I.; Beattie, N. A.; Macgregor, S. A.; Weller, A. S., Fluoroarene Complexes with Small Bite Angle Bisphosphines: Routes to Amine–Borane and Aminoborylene Complexes. *Eur. J. Inorg. Chem.* **2017**, *2017*, 4533–4540.

(11) Dallanegra, R. Cationic Rhodium Complexes with Chelating Phosphine and Phosphine Alkene Ligands. Application in Dehydrogenation and Dehydrocoupling Reactions. University of Oxford, Oxford, 2011.

(12) Kumar, A.; Beattie, N. A.; Pike, S. D.; Macgregor, S. A.; Weller, A. S., The Simplest Amino-Borane $H_2B{=}NH_2$ Trapped on a Rhodium Dimer: Pre-Catalysts for Amine–Borane Dehydropolymerization. *Angew. Chem. Int. Ed.* **2016**, *55*, 6651–6656.

(13) Adams, G. M.; Chadwick, F. M.; Pike, S. D.; Weller, A. S., A CH_2Cl_2 complex of a [Rh(pincer)]+ cation. *Dalton Trans.* **2015**, *44*, 6340–6342.

(14) Bruno, I. J.; Cole, J. C.; Edgington, P. R.; Kessler, M.; Macrae, C. F.; McCabe, P.; Pearson, J.; Taylor, R., New software for searching the Cambridge Structural Database and visualizing crystal structures. *Acta Cryst.* **2002**, *B58*, 389–397.

(15) Groom, C. R.; Bruno, I. J.; Lightfoot, M. P.; Ward, S. C., The Cambridge Structural Database. *Acta Cryst.* **2016**, *B72*, 171–179.

(16) The CSD searches were conducted using the ConQuest package (August 2018).

(17) Frisch, M. J.; Trucks, G. W.; Schlegel, H. B.; Scuseria, G. E.; Robb, M. A.; Cheeseman, J. R.; Montgomery, J., J. A.; Vreven, T.; Kudin, K. N.; Burant, J. C.; Millam, J. M.; Iyengar, S. S.; Tomasi, J.; Barone, V.; Mennucci, B.; Cossi, M.; Scalmani, G.; Rega, N.; Petersson, G. A.; Nakatsuji, H.; Hada, M.; Ehara, M.; Toyota, K.; Fukuda, R.; Hasegawa, J.; Ishida, M.; Nakajima, T.; Honda, Y.; Kitao, O.; Nakai, H.; Klene, M.; Li, X.; Knox, J. E.; Hratchian, H. P.; Cross, J. B.; Bakken, V.; Adamo, C.; Jaramillo, J.; Gomperts,

R.; Stratmann, R. E.; Yazyev, O.; Austin, A. J.; Cammi, R.; Pomelli, C.; Ochterski, J. W.; Ayala, P. Y.; Morokuma, K.; Voth, G. A.; Salvador, P.; Dannenberg, J. J.; Zakrzewski, V. G.; Dapprich, S.; Daniels, A. D.; Strain, M. C.; Farkas, O.; Malick, D. K.; Rabuck, A. D.; Raghavachari, K.; Foresman, J. B.; Ortiz, J. V.; Cui, Q.; Baboul, A. G.; Clifford, S.; Cioslowski, J.; Stefanov, B. B.; Liu, G.; Liashenko, A.; Piskorz, P.; Komaromi, I.; Martin, R. L.; Fox, D. J.; Keith, T.; Al–Laham, M. A.; Peng, C. Y.; Nanayakkara, A.; Challacombe, M.; Gill, P. M. W.; Johnson, B.; Chen, W.; Wong, M. W.; Gonzalez, C.; Pople, J. A. Gaussian 03, Revision D.01, Gaussian, Inc.: Wallingford CT, 2004.

(18) Becke, A. D., Density–functional exchange–energy approximation with correct asymptotic behavior. *Phys. Rev. A* **1988**, *38*, 3098–3100.

(19) Perdew, J. P., Density–functional approximation for the correlation energy of the inhomogeneous electron gas. *Phys. Rev. B* **1986**, *33*, 8822–8824.

(20) Andrae, D.; Häußermann, U.; Dolg, M.; Stoll, H.; Preuß, H., Energy–adjusted ab initio pseudopotentials for the second and third row transition elements. *Theor. Chim. Acta* **1990**, *77*, 123–141.

(21) Höllwarth, A.; Böhme, M.; Dapprich, S.; Ehlers, A. W.; Gobbi, A.; Jonas, V.; Köhler, K. F.; Stegmann, R.; Veldkamp, A.; Frenking, G., A set of d–polarization functions for pseudo–potential basis sets of the main group elements Al–Bi and f–type polarization functions for Zn, Cd, Hg. Chem. *Phys. Lett.* **1993**, *208*, 237–240.

(22) Hehre, W. J.; Ditchfield, R.; Pople, J. A., Self–Consistent Molecular Orbital Methods. XII. Further Extensions of Gaussian–Type Basis Sets for Use in Molecular Orbital Studies of Organic Molecules. *J. Chem. Phys.* **1972**, *56*, 2257–2261.

(23) Hariharan, P. C.; Pople, J. A., The Influence of Polarization Functions on Molecular Orbital Hydrogenation Energies. *Theor. Chim. Acta* **1973**, *28*, 213–222.

(24) Bader, R. F. W., Atoms in Molecules – A Quantum Theory. Oxford University Press: Oxford, 1990.

(25) Keith, T. A. AIMAII (Version 13.02.26, Professional), TK Gristmill Software (aim.tkgristmill.com): Overland Park KS, USA, 2015.

(26) Cosier, J.; Glazer, A. M., A nitrogen–gas–stream cryostat for general X–ray diffraction studies. *J. Appl. Crystallogr.* **1986**, *19*, 105–107.

(27) Oxford Diffraction Ltd.

(28) Sheldrick, G. M., SHELXT – Integrated space–group and crystal–structure determination. *Acta Cryst.* **2015**, *A71*, 3–8.

(29) Sheldrick, G. M., Crystal structure refinement with SHELXL. *Acta Cryst.* **2015**, *C71*, 3–8.

(30) Dolomanov, O. V.; Bourhis, L. J.; Gildea, R. J.; Howard, J. A. K.; Puschmann, H., OLEX2: a complete structure solution, refinement and analysis program. *J. Appl. Crystallogr.* **2009**, *42*, 339–341.